

Lynn El Ahmar

Characterization of Karst Geometry and Stability Analysis of Cave Tunnels in Bahia, Brazil

Characterization of Karst Geometry and Stability Analysis of Cave Tunnels in Bahia, Brazil

By

Lynn El Ahmar

in partial fulfilment of the requirements for the degree of

Master of Science
in Applied Earth Science

at the Delft University of Technology,
to be defended publicly on Thursday October 31, 2019 at 2:00 PM.

Supervisor:	Prof. Dr. G. Bertotti	TU Delft
Thesis committee:	Dr. J. K. Blom	TU Delft
	Dr. R. Lindenbergh	TU Delft

An electronic version of this thesis is available at <http://repository.tudelft.nl/>.

Acknowledgments

As this Masters study journey comes to an end, I look back at this unforgettable experience and can't but feel grateful for the immense academic and personal growth that I have gained during this phase of my life.

First, I would like to offer my sincere gratitude to supervisor Prof. Giovanni Bertotti for his constructive guidance and dedication throughout the course of this research project. His knowledge and expertise as well as his regular feedback and advice have helped me improve both academically and personally. Big thanks to PhD student Stephan De Hoop for always dedicating time to follow up and make sure I was on the right track.

This project is in consortium with UFRN (Universidade Federal do Rio Grande do Norte) and funded by Shell. Part of the project was also developed in collaboration with another Msc colleague Hanif Dinul Islam. Thanks to PhD student from Brazil Cayo Pontes for sharing his structural data. Also, thanks to PhD student Rahul Prabhakaran who took part of the acquisition of the LIDAR data along with Stephan.

I would also like to thank my thesis committee Dr. Roderik Lindenbergh and Dr. Jan Kees Blom for their time and assistance.

To my friend Ibrahim Mikati, thank you for making Netherlands feel a bit like home, also for your advice and continuous moral support.

Finally, I would have never had this opportunity to begin with if it wasn't for the support of my family. I love you more than words can ever say, and I am very much grateful for your continuous support of me towards achieving my goals. To the great man in my life, Tarek, thank you for keeping me going at times I felt like giving up. You inspire me and I admire you deeply.

*L. El Ahmar
Delft, October 2019*

Contents

List of Figures	viii
List of Tables	ix
Nomenclature	x
Abstract	xii
Introduction	1
1.1. General Overview	1
1.2. Research Objective	1
Literature Review	3
2.1. Regional Geology	3
2.2. Hypogene Speleogenesis	5
Methodology	8
3.1 Data Acquisition	8
3.2 Point Cloud Data Processing and Alignment	9
3.3 Metrics to Characterize Network Geometries	11
3.3.1 Conduit Shape & Aspect Ratio	11
3.3.2 Conduit Orientation	12
3.4 Structural Analysis	13
3.5 Stability Analysis	14
Results & Discussions	19
4.1 Point Cloud Data Processing and Alignment	19
4.2 Geometry Analysis	20
4.2.1 Conduits Shape and Aspect Ratio	20
4.2.2 Conduits Orientation	27
4.2.3 Discussion	29
4.3 Structural Analysis	30
4.4 Stability Analysis	31
4.4.1 Numerical Simulation Results	31
4.4.2 Sensitivity of parameters	36
4.4.3 Discussion	37
Conclusion	40
5.1 Conclusion	40
5.2 Recommendations	40
Bibliography	42
Appendices	44
Appendix 1. Cave Maps	44
Appendix 2. Cave Point Clouds Alignment	46
Appendix 3. Aspect Ratios	50
Appendix 4. Structural Data	52
Appendix 5. Stability Analysis Contour Plots	57

List of Figures

Figure 1. Localization map of the study area and geological setting of the Irece basin within the Sao Francisco Craton.	4
Figure 2. Satellite image showing localization map of the studied caves (Google Earth)	4
Figure 3. Conceptual model of typical types of hypogene caves based on geological structure and type of flow (Audra 2007, Audra et al. 2009a, b)	5
Figure 4. Conceptual model of the morphologic suite of rising flow (<i>MSRF</i>) which is diagnostic of rising cave-forming fluid flow in hypogene speleogenesis (Klimchouk et.al, 2016)	6
Figure 5. Mobile LiDAR device used for the cave scanning (ZEB-REVO GeoSLAM)	8
Figure 6. Scanned cave interior of <i>TOR</i> shown in 3D point cloud (Hoop, 2018)	9
Figure 7. Point cloud registration using rotation and translation based on observation of overlapping points	10
Figure 8. Comparison of the <i>TOR</i> point cloud with the 2D cave map	11
Figure 9. Representation of the equation of the aspect ratio of an ellipse	12
Figure 10. Example showing the rules used for generating the skeleton of the cave bodies	12
Figure 11. Map view of cave Lapinha as (left) point cloud (right) converted to a schematic map with skeleton for geometrical analysis based on the stated rules	13
Figure 12. (A) Schematic map of Lapinha cave showing the cave skeleton with linear segments. (B) Cyclic structures in case of passage loops due to epigenic stalagmites/stalactites	13
Figure 13. Discretization in the Boundary Element Method for 3D unbounded problem (Hamdan, 2013)	14
Figure 14. Point cloud alignment of <i>DDM</i> cave	19
Figure 15. Point cloud alignment of <i>TOR</i> cave. Location in the box denotes the maze network with insufficient point density	20
Figure 16. Cross sections and aspect ratio measurements with distance of <i>DDM</i> cave	21
Figure 17. Cross sections and aspect ratio measurements with distance of <i>IOI</i> cave	22
Figure 18. Change of width of <i>IOI</i> passage moving from cross section 3 till 10	22
Figure 19. Illustration showing the geometry corresponding to changes in water table fed by deep rifts. Right diagram shows the rift gradually narrowing away from the feeder (Audra, 2019)	23
Figure 20. Boundary between two parts of the cave with different characteristics	24
Figure 21. Cross sections and aspect ratio measurements with distance of <i>TOR-Part A</i>	24
Figure 22. Cross sections and aspect ratio measurements with distance of <i>TOR-Part B</i>	25
Figure 23. Cross sections and aspect ratio measurements with distance of <i>TOR-Part B Maze 1</i>	25
Figure 24. Cross sections of <i>TOR-Part B Maze 2</i>	25
Figure 25. Cross sections of <i>LAP</i> cave	26
Figure 26. Cross sections and aspect ratio measurements with distance of <i>PAX</i> cave	27
Figure 27. Orientation analysis of <i>DDM</i> cave showing a single preferential orientation	28
Figure 28. Orientation analysis of <i>IOI</i> cave showing a single preferential orientation	28
Figure 29. Orientation analysis of <i>TOR</i> cave showing two preferential orientations perpendicular to each other	28
Figure 30. Orientation analysis of <i>LAP</i> showing two preferential orientations perpendicular to each other	29
Figure 31. Orientation analysis of cave Paixao showing a dominant single orientation	29
Figure 32. Rose diagrams showing orientations of fractures, vein and conduits in all of the caves	30
Figure 33. Contour plot of spalling criterion values for tunnel 1 showing how width and height of the critical zone are measured based on spalling values greater than 4	32
Figure 34. Width of deformed zones horizontally from the tunnel boundary with depth for the different tunnels	33
Figure 35. Comparison of maximum shear strain values for tunnels with different aspect ratios	33
Figure 36. Plot showing the effect of changes in tunnel dimension compared to changes in the aspect ratio. Note that there are two x-axes in the plot, the top refers to tunnel dimension and the bottom one refers to the aspect ratio	34
Figure 37. Estimated minimum depth of collapse potential for the different tunnel geometries with respect to aspect ratio	35
Figure 38. Comparison between a rectangular and ellipse geometry stability for different aspect ratios	35
Figure 39. Sensitivity analysis of overburden	36
Figure 40. Sensitivity analysis of tensile strength	36
Figure 41. Sensitivity analysis of cohesion	37
Figure 42. Sensitivity analysis of friction angle	37

List of Tables

Table 1. Point Cloud Data of the 3D LiDAR surveys acquired.....	9
Table 2. Cave cross sections used for the numerical modelling.....	16
Table 3. Rock Mechanical properties used for the numerical modelling.....	16
Table 4. Rock Mass Strength parameter values used for sensitivity analysis.....	17
Table 5. Main conduit shapes observed in the geometry analysis of the caves.....	20
Table 6. Critical zone dimensions for the different tunnel slices at a depth of 500m.....	32
Table 7. Minimum depth of collapse potential for the different tunnel slices.....	34

Nomenclature

DDM	Diva De Maura
IOI	Ioio
TOR	Torrinha
LAP	Lapinha
PAX	Paixáo
MSRF	Morphologic Suite of Rising Flow
LIDAR	Light Detection and Ranging
ICP	Iterative Closest Point
SLAM	Simultaneous Location and Mapping
CRS	Coordinate Reference System
BEM	Boundary Element Method
UCS	Unconfined Compressive Strength
σ_1	Maximum In-Plane Principal Stress
σ_3	Minimum In-Plane Principal Stress
e_{max}	Maximum Shear Strain
e_1	Major In-Plane Strain
e_3	Minor In-Plane Strain

Abstract

Carbonate reservoirs are of significant importance as they host a high percentage of the world's oil and gas reserves. They are however subject to dissolution and may be heavily karstified often resulting in large cavities which may impose major hazards in drilling and production. In many cases, difficulty remains due to poor understanding of karst geometry and how it is distributed. This research presents a geometry and stability analysis using LIDAR (Light Detection and Ranging) data on cave systems in Brazil that can serve as direct analogues to subsurface carbonate reservoirs and therefore enhance our ability to predict them. Our study area lies in the state of Bahia in Brazil and consists of five caves: Diva De Maura, Torrinha, Ioiô, Lapinha, and Paixão. These cave systems occur in Neoproterozoic carbonates of the Salitre Formation in the Irecê basin of the São Francisco Craton. Analysis of the geometry shows existing preferential karstic developments and tunnel shape patterns mainly classified in two, horizontal ellipse and vertical ellipse. Analysis of geologic structures and orientations of cave passages show that these caves exhibit marked structural guidance with two main orientations N-S and E-W. This aligns with the regional phases of deformation corresponding to collisional events that occurred on the margin of the São Francisco Craton. Stability analysis shows that tunnels aspect ratio is a major parameter controlling the stability, whereas the dimension of a tunnel has a much less effect on stability. Tunnels with aspect ratios less than 1 show a collapse depth greater than 1000 m and are more stable than tunnels with aspect ratios greater than 1. Results show that almost all tunnels with a horizontal ellipse geometry are supported with rock that is already undergoing severe deformation at a depth of 500m. Sensitivity tests show that overburden and rock mass strength parameters namely cohesion have the largest effect on the stability results.

Introduction

1.1. General Overview

Studying carbonate reservoirs is highly important as it is believed that carbonates host ~ 50 % of the world's oil and gas much of which is trapped in karstic porosity (Ford, 2007). Carbonates are however subject to what is termed as karstification, which is a complex that depends on several factors such as fluid-rock interaction, lithology and, the geologic structure. Karstification occurs with widespread dissolution of the host rock and therefore creates some large cavities. Though presence of such cavities helps enhance permeability, on the other hand it imposes some major problems related to drilling and the reservoir stability. We therefore expect significant challenges and technical risks accompanied with the production from carbonate reservoirs, especially owing to the highly complex internal structure of karst and the difficulty in understanding how it is distributed in the subsurface.

Brazil is home to large areas of carbonate karsts estimated at 5 to 7 % (425,000-600,000 km²) of the total surface of the country (Karmann, 1994) which makes it an important target for research on karsts. Not only carbonate areas in Brazil are extensive but the access to these areas is fairly easy due to very little or no relief and well populated areas (Auler, 2002). The most extensive karst regions occur in central Brazil in rocks of the Bambuí and Una Groups (Auler, 1996). The identification of the type of speleogenesis and the processes that govern the formation and distribution of karst in a cave is highly essential for carbonate reservoir characterization. The challenge that accompanies the exploitation of such reservoirs is mainly due to the poor understanding of the karst systems. A detailed study of accessible caves is therefore a necessity as they represent direct analogues of karst reservoirs in the subsurface and provide insight on reservoir porosity and permeability distribution as well as subsequent fluid flow.

1.2. Research Objective

This study is focused on cave systems of the Irecê basin consisting of the Diva De Maura, Torrinha, Ioiô, Lapinha, and Paixão caves of which some are of hypogene origin and others of epigene origin. The aim is to understand the geometry of these cave systems while taking their underlying speleogenetic processes into account, their interrelation with fracture networks, along with the stability aspect to better characterize carbonate reservoirs for further implement in oil exploitation. For that purpose, the present study is based on the use of 3D LIDAR data of the cave interior to extract a set of metrics that could aid in constraining factors controlling the geometry of those caves. A stability analysis is then done to compare to investigate collapse potential and compare between the different geometries.

Literature Review

2.1. Regional Geology

The study area lies in the Irecê basin of the São Francisco Craton, Brazil (figure 1,2). It is located towards the northern part of the São Francisco Craton on which an extensive carbonate platform had formed during the Late Proterozoic. This sedimentary terrain consisted of carbonates of the Una and Bambuí Groups overlying Paleo-Mesoproterozoic sedimentary and Archean metamorphic units (Misi et al., 2011). The Una Group comprises two formations, the Bebedouro and Salitre Formations. The Bebedouro Formation, constituting of glacio-marine sediments, formed during a major glacial event that had affected the craton at approximately 1 Ga. In the period between 750 and 650 Ma, the Salitre Formation deposited with thickness of hundreds of meters. Most of the cave systems in Brazil are formed in the Salitre Formation thus it is our main target for investigation.

The São Francisco Craton is bordered by the Brasília, Rio Preto, Riacho do Pontal, Sergipano, and the Aracuai fold belts as seen in figure 1. The tectonic evolution of the Neoproterozoic sedimentary basins in that region started in response to extensional events during the fragmentation of Rodinia. Later tectonic inversion and compressional movement developed the São Francisco basin which lies west to the Irecê basin (see figure 1). The Irecê basin is likely to have formed in response to the same tectonic events that formed the São Francisco basin (Misi and Kyle, 1994). Deformations in the Neoproterozoic units of these basins have also been influenced by the collisions between the São Francisco Craton and the bordering fold belts. According to a structural analysis done by Ennes-Silva, there has been evidence of superposed folding on the Neoproterozoic sedimentary units. It was shown that these units exhibit two phases of deformation. The first are folds and thrusts striking NNE-SSW and the second are folds and thrusts striking E-W, both of which correspond to collisional events that occurred on the margin of the craton (Ennes-Silva et al., 2015).

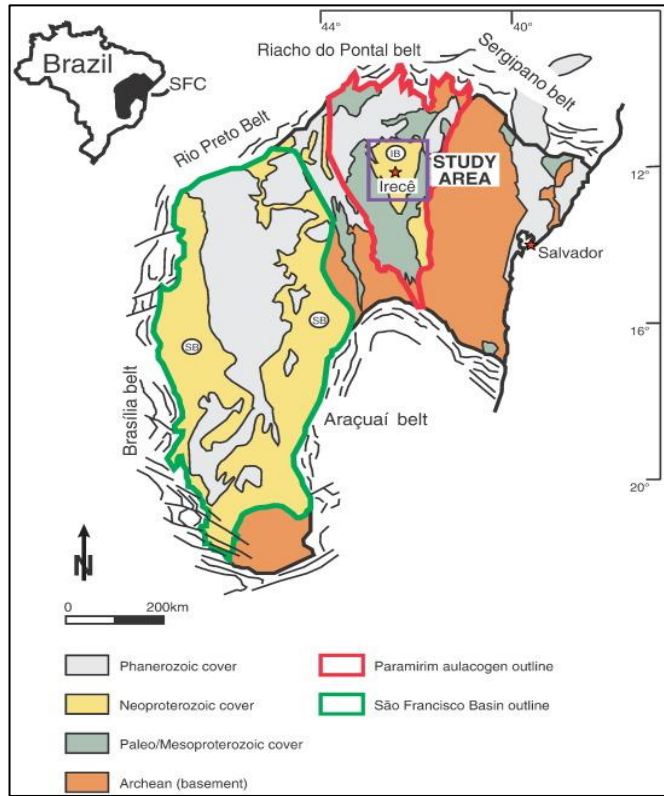


Figure 1-Localization map of the study area and geological setting of the Irecé basin within the Sao Francisco Craton.

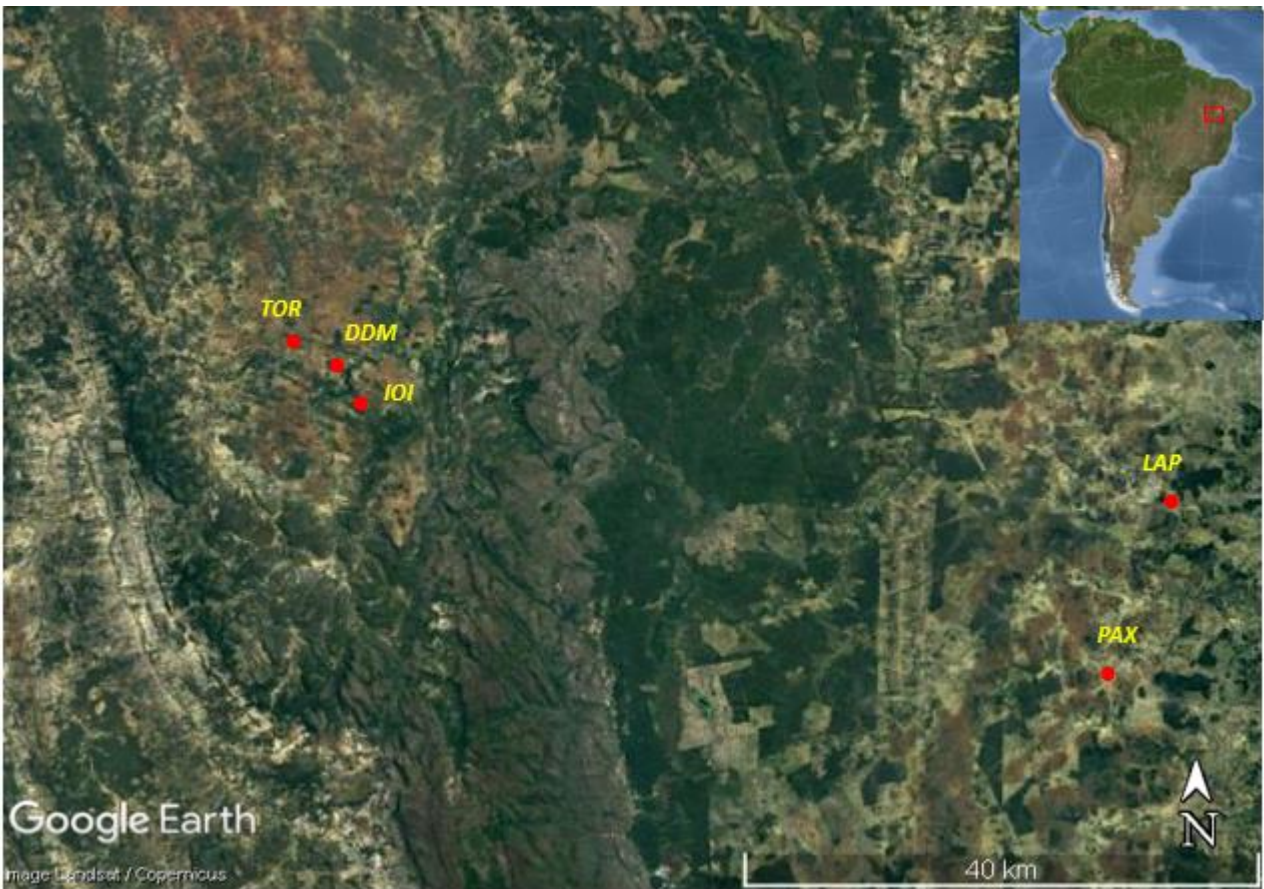


Figure 2- Satellite image showing localization map of the studied caves (Google Earth).

2.2. Hypogene Speleogenesis

Speleogenesis is the development of well-organized cave systems by fluids moving through fissures of a soluble rock (Audra, Palmer, 2015). Traditionally caves have been classified as epigenic where dissolution of exposed carbonate rocks occurs due to released carbonic acid by reactions with CO₂ in soil upon the infiltration of meteoric water. The advancements in the study of karsts led to the growing recognition of the widely occurring hypogenic caves where karsts form in deep seated conditions and thus have no linkage to the surface. It has been clear that certain features and patterns show evidence of upward movement of deep water that differs fundamentally from surface-related epigene features. Hypogene speleogenesis is therefore defined as “the formation of solutionally enlarged permeability structures by the upwelling groundwater flow, independent of recharge from the overlying or immediately adjacent surface” (Klimchouk, 2015).

The uprising fluids could be driven by hydrostatic pressure or possibly by thermal or concentration gradients. The resulting patterns are often complex and are guided by the permeability structure of the soluble host rock which is why hypogene processes are often heavily influenced by the fracture patterns in the rock. The hypogene flow often develops network maze patterns which may either be systematic or polygonal depending on the nature of the fracture networks (Klimchouk et.al, 2016). A conceptual model of the most typical hypogene cave patterns is shown in figure 3. Patterns are mainly subdivided into two types: deep phreatic systems which are generally developed in confined aquifers by transverse speleogenesis, and systems developed above the water table where condensation-corrosion plays an important role (Audra, 2017).

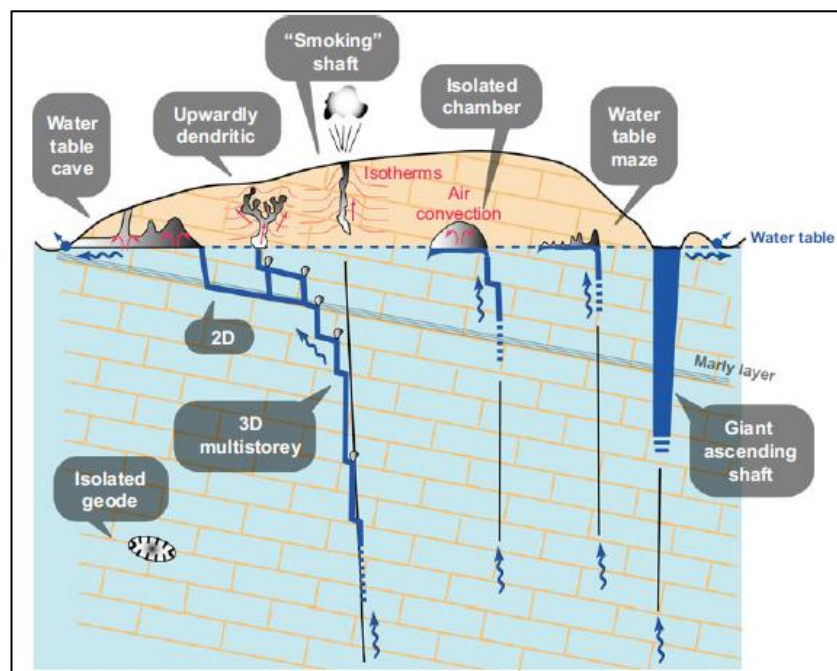


Figure 3-Conceptual model of typical types of hypogene caves based on geological structure and type of flow (Audra 2007, Audra et al. 2009a, b).

Certain arrangements of individual features characterize what is distinguished as the morphologic suite of rising flow (MSRF; Klimchouk, 2007, 2009). This often shows a regular combination of features through which ascending fluid flow can be traced from rising inlet features (termed feeders, vents, or risers), through transitional wall and ceiling features, to spherical ceiling pockets (cupolas) and outlet features (domepits) (Klimchouk et.al, 2015). This arrangement provides diagnostic evidence of hypogene speleogenesis and has been recognized in hundreds of hypogene caves across the globe (Klimchouk et.al, 2016). Figure 4 shows the conceptual representation of the morphologic suite of rising flow in hypogene systems.

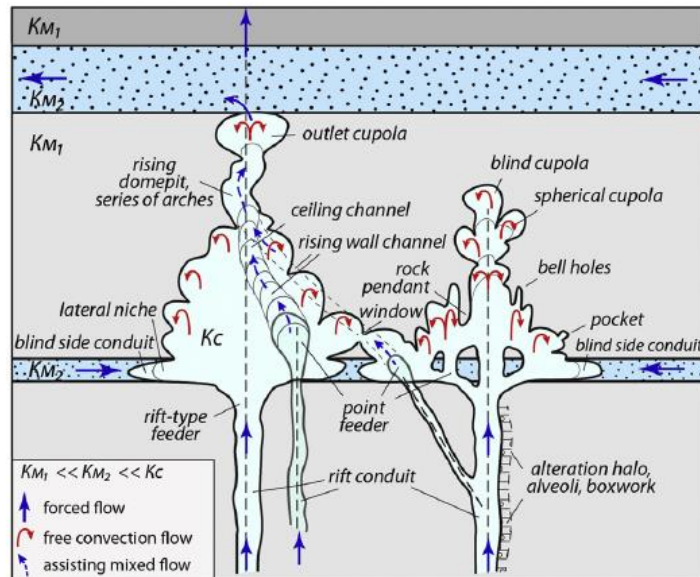


Figure 4- Conceptual model of the morphologic suite of rising flow (MSRF) which is diagnostic of rising cave-forming fluid flow in hypogene speleogenesis (Klimchouk et.al, 2016)

Methodology

3.1 Data Acquisition

Earlier attempts to quantitatively characterize karst networks have been mainly based on conventional methods of hand mapping and creating two-dimensional planar maps. Not only this mapping technique is very tedious and time consuming, but depends on manual measurements which is certainly prone to human errors besides the fact that it is only in 2D. 3D LiDAR surveying has recently emerged as a new tool that eases the acquisition process and storage of the acquired data and achieves scan results with high accuracy (Zlot and Bosse, 2014b). In this study we rely on 3D LiDAR data which was acquired in a 2018 campaign in the caves of Brazil to obtain the information needed to quantitatively characterize karst networks in that area.



Figure 5- Mobile LiDAR device used for the cave scanning (ZEB-REVO GeoSLAM).

A mobile LIDAR device, Geoslam ZEB REVO®, was used to obtain point clouds of the cave interior geometry (figure 5). This handheld device makes it quite easy to map a cave interior as it only requires a single operator holding it while traversing a cave. The device uses SLAM (Simultaneous Location and Mapping) based scanner with a rotating laser that captures real time point clouds up to a centimeter accuracy while the operator is moving. Prior planning of a survey path is required in order to decide on a stationary location that marks the initialization and the end of the survey. This is done for loop closure in order to minimize drift in the solution (Zlot and Bosse, 2014b). The data that is recorded after the device has been initialized is stored in a data logging unit as the operator walks the trajectory. The raw data that is acquired is then transferred from the data logger and converted into metrically accurate 3D point clouds for further processing (figure 6 shows an example of cave interior in point cloud).

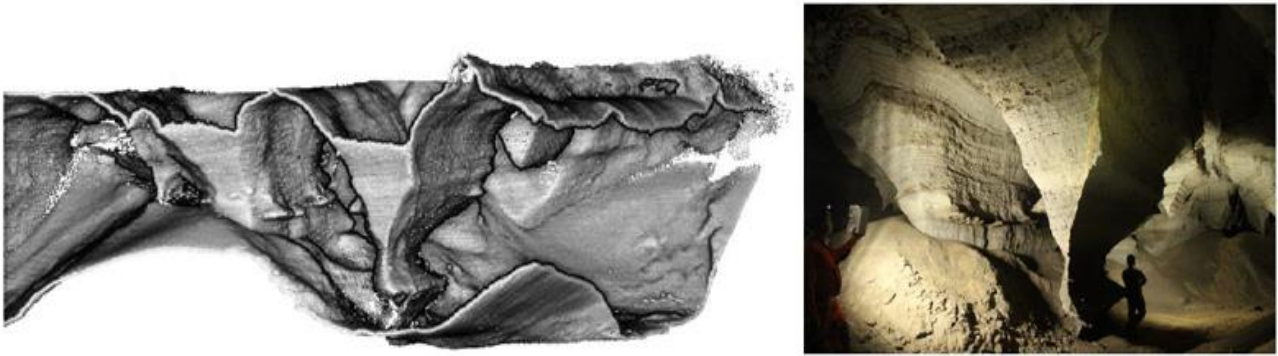


Figure 6-Scanned cave interior of *TOR* shown in 3D point cloud (Hoop, 2018).

3.2 Point Cloud Data Processing and Alignment

Due to the normally challenging environment in caves with possibly difficult terrain, in some cases, splitting up the surveys is necessary to be able to safely traverse the cave. Since such difficulty was encountered in some parts during the acquisition, each cave was surveyed in multiple segments; hence processing the data required point cloud registration steps in order to align the surveys together (point cloud data seen in table 1) A 3D point cloud processing software *CloudCompare* was used to process the LIDAR surveys. For the purpose of point clouds alignment, the software had several ways to perform this task which were all tested to check for best results. What is meant by point cloud alignment is stitching (registering) two point clouds based on overlapping points; best results are judged based on how minimal the offset between the point clouds is upon registration.

Table 2- Point Cloud Data of the 3D LiDAR surveys acquired.

Cave	Number of Surveys	Total Points
<i>DDM</i>	4	43,391,767
<i>IOI</i>	4	35,911,676
<i>TOR</i>	4	70,957,043
<i>LAP</i>	2	36,239,534
<i>PAX</i>	2	50,295,335

The easiest way through which we were able to achieve desirable results was simply performing a manual transformation where one cloud is taken as a *model cloud* (reference) and the other is taken as a *data cloud* (one which will be moved). Afterwards rotation and transformation are applied to the *data clouds* with respect to the reference based on our observations of obvious overlapping points (figure 7). Another method which we tried but found to be less reliable than the manual transformation is the point pairs picking method where the user picks several equivalent points from each cloud and then the tool automatically registers the clouds together. It was rather a less efficient method and took some effort to pick the proper points that would achieve better registration of the clouds. Results still showed obvious offset between the point clouds. The last one was an automatic method known as the *Iterative Closest Point* (ICP) algorithm; this algorithm iteratively estimates the combination of rotation and translation needed based on a root mean square point to point distance metric minimization technique. This method was used to check if better results are achieved (less offset between the registered point clouds) after the manual transformation; however little if any enhancement was observed so we ignored it since sometimes it required additional steps involving weighing points and

rejecting outliers before alignment. The manual transformation method was therefore the simplest yet yielding successful results with barely any noticeable offset between the registered point clouds.

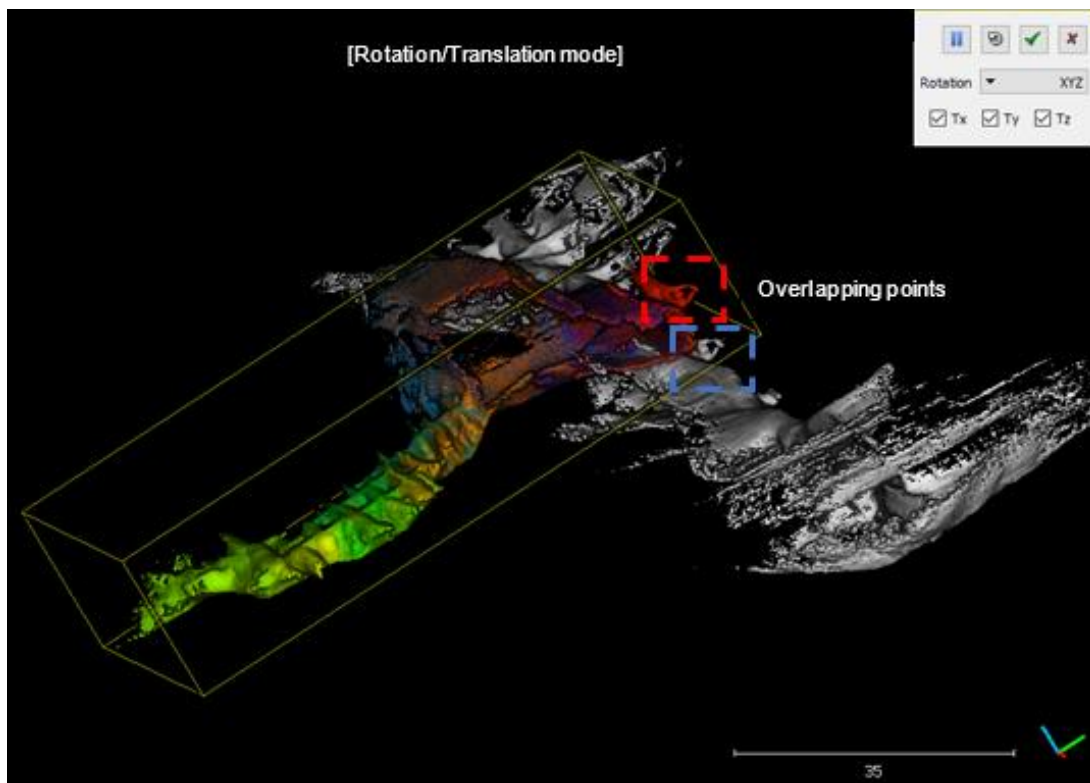


Figure 7-Point cloud registration using rotation and translation based on observation of overlapping points.

Afterwards the aligned point clouds of the caves are compared with the 2D maps of those caves which were previously made by Grupo Bambui de Pesquisas Espeleológicas (figure 8). Results of the aligned cave point clouds along with the 2D maps are found in Appendix 1 and 2.

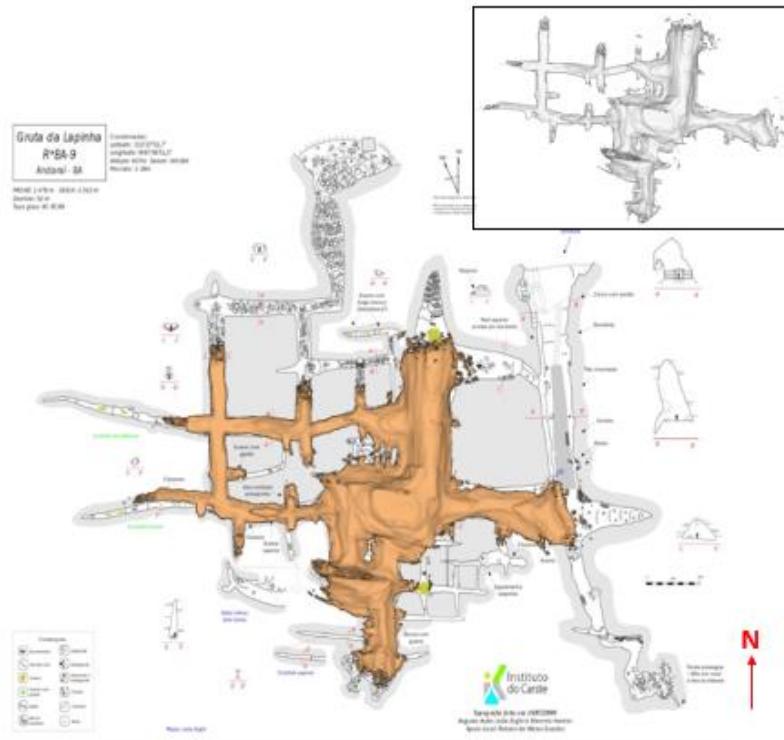


Figure 8-Comparison of the TOR point cloud with the 2D cave map.

3.3 Metrics to Characterize Network Geometries

Point clouds as processed in CloudCompare have only local coordinates and are not geo-referenced which makes it difficult to be able to extract useful parameters such as real distances between tunnels, lengths and other statistical metrics needed for the geometrical analysis of karst networks. They are therefore converted into georeferenced graphs through QGIS software for real distance computations. The process to that includes extracting the local coordinates of the points from CloudCompare as $\{x,y,z\}$ coordinates. Due to the very large number of data points in a survey which cannot be entirely extracted into a document or excel file, a Python script is used to down sample the number of points whereby an iteration is applied to extract every 100th or 50th point so that the total number of points is largely reduced. QGIS then allows us to define for this data a global and project-wide coordinate reference system (CRS) in which case WGS 84 / Pseudo-Mercator projection is used. This CRS projection is suitable for use in world between 85.06°S and 85.06°N. Upon defining the coordinate system, x and y coordinates of the points are then used to display a planar 2D map of the caves above which layers can be added to manually draw a graphical representation (figure 11).

3.3.1 Conduit Shape & Aspect Ratio

Shapes of conduits are investigated to determine any existing patterns attributed to certain areas or orientations. The shapes of the conduits are observed on the 3D point clouds and cross sections in the vertical direction which are mostly representative of the tunnel's shape are taken. Those cross sections are then imported as *ASCII text* files into QGIS for real distance measurements. Measurements of the widths and the lengths of the tunnels are recorded to get an aspect ratio value (figure 9).

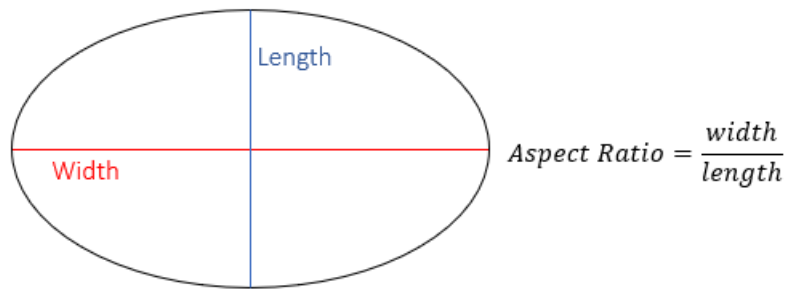


Figure 9-Representation of the equation of the aspect ratio of an ellipse.

3.3.2 Conduit Orientation

To analyse network geometry of caves it is of relevance to compute the conduits orientation. For that purpose, we first produce a skeleton of the caves with a set of nodes connecting segments based on the geometry of the karst network. For simplicity nodes are only placed at the end of segments and the intersection point between two segments. The skeleton is kept as simple as possible and of course preserving the topology of the caves. Certain rules have been used consistently as a basis for generating the skeletons (figure 10):

1. Segments are drawn only when a conduit length is greater than 4% of the main conduit's length.
2. A new segment is drawn only when there is a change in orientation that is greater than 5 degrees.
3. Epigenetic features such as stalagmites and stalactites which in some cases appear as passage barriers are not taken into account as these may have occurred in later stages and thus have no linkage to the origin of caves (figure 12).

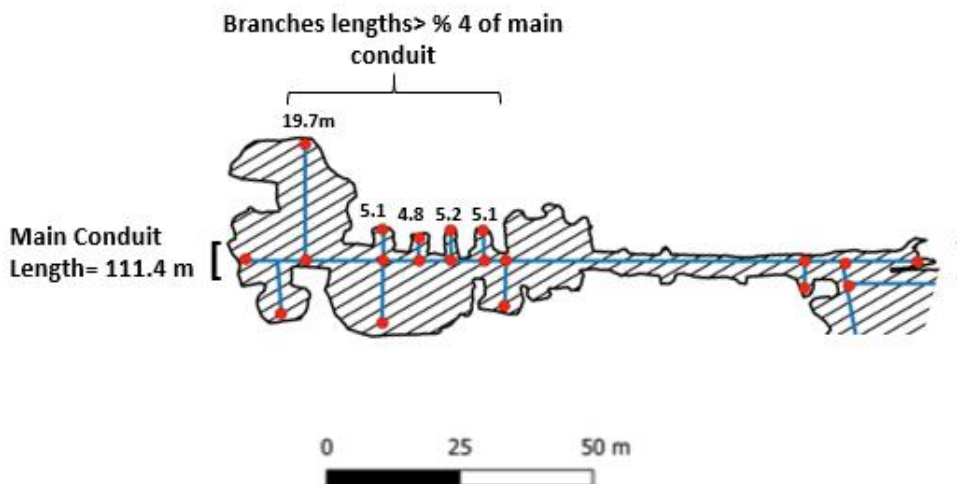


Figure 20-Example showing the rules used for generating the skeleton of the cave bodies.

Conduit orientations are then computed based on the skeletonized graphs of the caves. Azimuth is measured as the angle between the north and the individual segment ranging from 0 to 360°. The orientation data is analysed on a Rose diagram that can depict clearly dominant orientations. Since the lengths of the segments vary, each orientation value is weighted by the length of the segment while computing a Rose diagram. This gives an estimate of the relative frequency of the preferred directions with respect to other less dominant directions. Computing conduits orientation and its distribution in the cave is certainly a useful parameter to assess the existence and relative importance of preferential karstic developments.

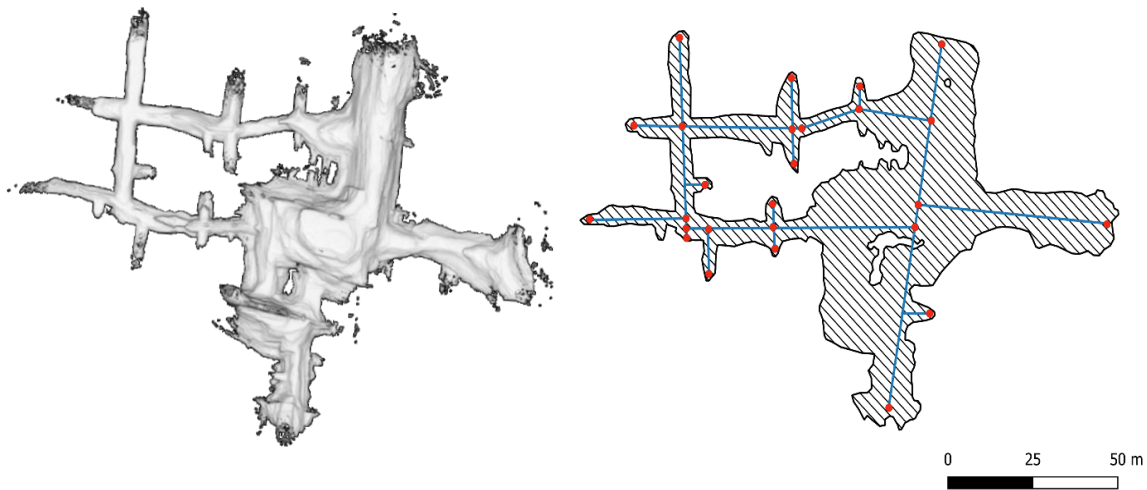


Figure 11-Map view of cave Lapinha as (left) point cloud (right) converted to a schematic map with skeleton for geometrical analysis based on the stated rules.

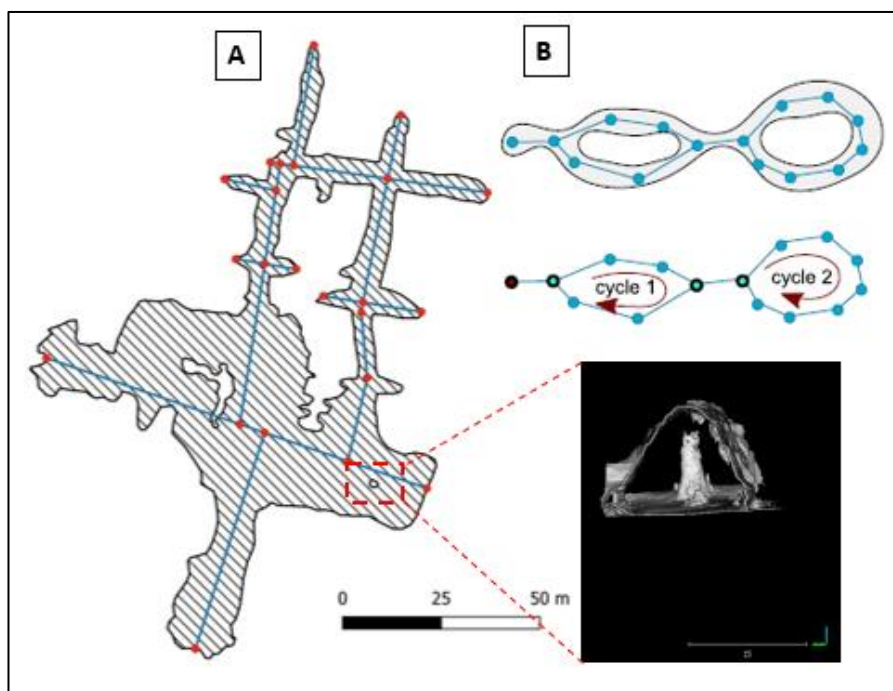


Figure 12-Passage loops due to epigenic features are not taken into account thus cyclic structures are not used while producing the cave skeleton. (A) Schematic map of Lapinha cave showing the cave skeleton with linear segments. (B) Cyclic structures in case of passage loops due to epigenic stalagmites/stalactites.

3.4 Structural Analysis

Some field structural data was provided by PhD student Cayo Pontes from the *Universidade Federal do Rio Grande do Norte*; this data is used is to make comparison between fracture networks and the conduit orientations in order to check the degree of correlation between both. The data is plotted on Rose diagrams using *Stereonet* and compared to the conduits orientation results.

3.5 Stability Analysis

Investigating stability of underground cavities invites many relevant researchers and practitioners into understanding rock mechanics related to increased stress in subsurface rocks. In our case it is particularly a concern due to the increase in stress levels introduced by drilling from reservoirs where such cavities are present and therefore the hazard which that would impose. Estimation of the failure pattern of caves under certain stress conditions would be essential in understanding their geomechanical stability. For this purpose, a numerical model for stress/strain analysis is adopted using the boundary element method (BEM) in order to analyze the response of these caves to different stress conditions. The BEM is a numerical technique for solving initial value problems based on an integral equation that is defined on the boundary of the domain and an integral that relates the boundary solution to the solution at points in the domain (www.boundary-element-method.com). It has the advantage that only the boundary of the domain needs to be meshed so therefore it is discretized into elements and the surrounding rock mass is treated as an infinite continuum (figure 13). Since discretization is required only along the boundary, this therefore leads to the reduction of the spatial distribution of our domain of interest by one. For example, an equation governing a three-dimensional region would then be transformed in two dimensions. Since fewer elements are required in this case, it makes it a less tedious technique compared to other techniques such as the finite element method where a significant amount of effort is required to generate a mesh first and then having the entire rock mass discretized into individual elements. Therefore, the BEM has been a very powerful numerical method due to its simplicity while still producing high accuracy stress analysis.

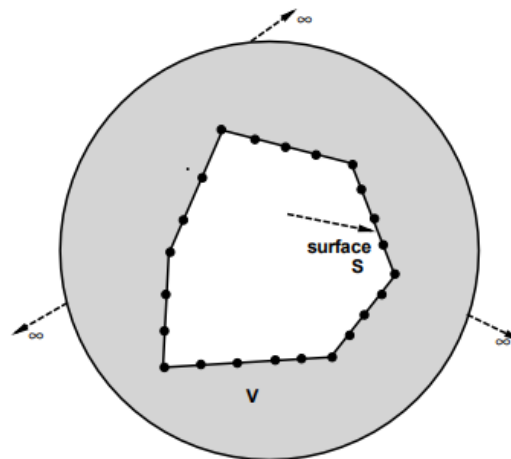


Figure 13-Discretization in the Boundary Element Method for 3D unbounded problem (Hamdan, 2013).

A boundary element software called *Examine2D* is used for the purpose of our analysis. It will be used to demonstrate the effect of differences in the tunnel geometries along with other rock parameters on the induced stresses and consequently failure patterns of the different cave tunnels. This software is convenient due to its capability for conducting real-time analysis which allows us to manipulate the model and directly view the influence of these changes. The assumptions used in this model are that the material being modeled is homogenous, isotropic, and linearly elastic. It is therefore important to note that this software is limited to elastic analyses thus the near field rock mass model may not be as precise after failure is attained (where elastic conditions no longer hold). Since *Examine2D* calculates only elastic displacements, this in reality may be quite a small part of the actual measured deformation in the field. As long as this effect is kept in mind, results can still yield useful information on behavioral trends of induced stress and strain in the plane of the analysis.

The software is based on plane strain conditions, whereby the principal stresses are defined in terms of in plane stresses σ_1 and σ_3 and out of plane stress σ_z . The software calculates σ_1 and σ_3 being the maximum

and minimum in plane principal stresses respectively. It is important to mention though that σ_1 may not necessarily be the maximum principal stress in 3D; if the out of plane σ_z is of greater value, then the in plane σ_1 would therefore be the intermediate principal stress in 3D. Likewise σ_3 may not necessarily be the minimum principal stress in 3D; if σ_z has a less value, then the in plane σ_3 would therefore be the intermediate principal stress.

The governing equations of the numerical modeling of the present study are the following:

$$\sigma_1 = \frac{\sigma_x + \sigma_y}{2} + \sqrt{\left(\frac{\sigma_y - \sigma_x}{2}\right)^2 + \tau_{xy}^2}$$

$$\sigma_3 = \frac{\sigma_x + \sigma_y}{2} - \sqrt{\left(\frac{\sigma_y - \sigma_x}{2}\right)^2 + \tau_{xy}^2}$$

maximum shear strain $e_{max} = e_1 - e_3$

Where e_1 and e_3 are the major and minor in-plane principal strains respectively.

Spalling Criterion equation: $\frac{\sigma_1 - \sigma_3}{UCS}$

Where UCS refers to unconfined compressive strength defined as the ultimate breaking strength of the rock. It is expressed as the maximum load at failure divided by the cross-sectional area.

For the present study, the Spalling Criterion is used to indicate failure in the cave tunnels. Spalling is a mode of damage defined as the development of visible extension fractures under compressive loading near the boundary of a tunnel (Diederichs, 2010), in other words it refers to the process of fracture initiation and propagation. As a general guideline, Spalling Criterion values less than 0.4 indicate no potential for failure to develop; values of 0.4 indicate initiation of damage such as onset of fracturing; and values of 0.7 and higher indicate potential for the occurrence of strain bursting (<http://www.rocscience.com>). Since most failure mechanisms in caves have been drawn from rock mechanics of mining excavations, the present study of caves instability will be based on failure criteria that is also applied for underground mines, instead we refer to failure in this case as ceiling collapse or, as termed, cave breakdown.

It is reasonable to mention though that caves are different than mines in that they have been excavated over a long period of time through slow dissolution rather than blasting. Stress patterns responsible for failure around these underground openings thus would be expected to be different. Horizontal strain in caves is most likely to have been annealed thus we would expect that only strain remaining is that due to the gravitational loading on caves ceilings (White, 2005). In this modeling we are assuming a scenario where vertical stress σ_v is much greater than the horizontal stress σ_h for all experiments. It is uncertain to know whether the horizontal strain due to tectonic deformation has been completely annealed. Many massive ceiling failures in limestone mines are thought to be due to compressive stresses parallel to the bedding (Esterhuizen et al., 2007). And it also has been observed that several residual cavities in mine collapses have some similarity to those in caves so it could be possible that similar failure mechanisms are responsible (White, 2005).

The stress and strain results upon the change in input parameters can be viewed by means of contour patterns surrounding the tunnels. Results of the modelling are presented in terms of two mechanical properties:

- Maximum shear strain, for the comparison of amount of deformation occurring for tunnels with different aspect ratios.
- Spalling Criterion values, for detection of damage zone and breakout potential.

Table 2-Cave cross sections used for the numerical modelling.

<i>Name</i>	<i>Cave</i>	<i>Shape</i>
Slice 1	Diva De Maura	
Slice 2	Torrinha	
Slice 3	Lapinha	
Slice 4	loio	
Slice 5	Paixão	

The numerical modelling is done on specific cross sections taken from each of the caves and that represent the main different geometries that were encountered in the previous analysis (table 2). To be able to make comparisons between responses of the different geometries, values of rock mechanical properties and other input parameters are fixed as shown in table 3.

Table 3-Rock Mechanical properties used for the numerical modelling.

Field Stress	Type	Gravitational Stress
	Ground Surface Elevation	500 (m)
	Overburden Unit Weight	0.021 (MN/m ³)
	Horizontal Stress Ratio	0.38
Rock Mass Elastic Properties	Type	Isotropic
	Young's Modulus	59000 (Mpa)
	Poisson's Ratio	0.275
Rock Mass Strength	Type	Mohr Coulomb
	Tensile Strength	2.75 (Mpa)
	Cohesion	15.16 (Mpa)
	Friction Angle	38.4 deg

Afterwards different modeling scenarios are used to demonstrate the effect of changes in input parameters as in the sensitivity of those parameters. The input parameters which will be tested are:

- Rock Mass Strength parameters (tensile strength, cohesion, friction angle)
- Overburden Unit Weight (based on density range for limestone)

The rock mass elastic properties (Young's modulus and Poisson ratio) showed little effect on the results so therefore will be kept constant throughout the analysis. Since values specific to the area of study are not available, for this present model we assume all the lithology is limestone and use mid values of ranges that are specific to limestone (according to Goodman 1989), table 4.

Table 4-Rock Mass Strength parameter values used for sensitivity analysis

	<i>Tensile Strength</i>	<i>Cohesion</i>	<i>Friction Angle</i>
<i>Low</i>	1.5	6.72	34.8
<i>Mid</i>	2.75	15.16	38.4
<i>High</i>	4	23.6	42

Results & Discussions

4.1 Point Cloud Data Processing and Alignment

Cave point clouds were aligned using manual rotation and transformation. Figures 14, 15 show the separate surveys before and after alignment of caves *DDM* and *TOR* (the other caves are found in the appendix). The process of manual transformation achieved good alignment results as mentioned earlier with barely any noticeable offset. The process took a lot of time however due to the large amount of points which was causing the software to respond very slow and crash several times therefore having to repeat the process all over again. Down-sampling of points could have maybe helped reduce this problem.

The GeoSlam device that was used for the acquisition of this data lacked a real-time datalogger which helps to simultaneously collect and process scanned data of the cave regions and control the point cloud density based on the areas of interest. Therefore, point cloud density in certain interesting locations was not enough which didn't make it possible to extract any measurements because the boundary of the tunnel is not complete. This is the case in for example one of the mazes in *TOR* (figure 15) which could not be investigated due to insufficient point density (examples of cross sections with insufficient point density are seen in the following section).

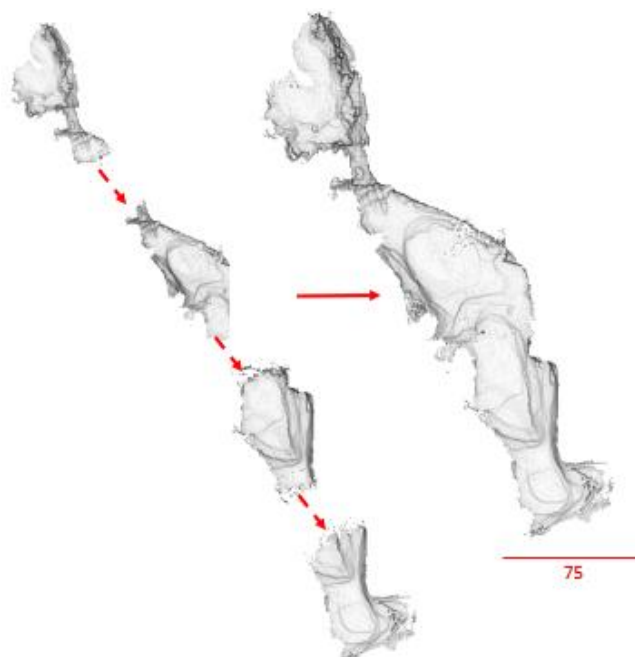


Figure 14-Point Cloud Alignment of *DDM* cave.

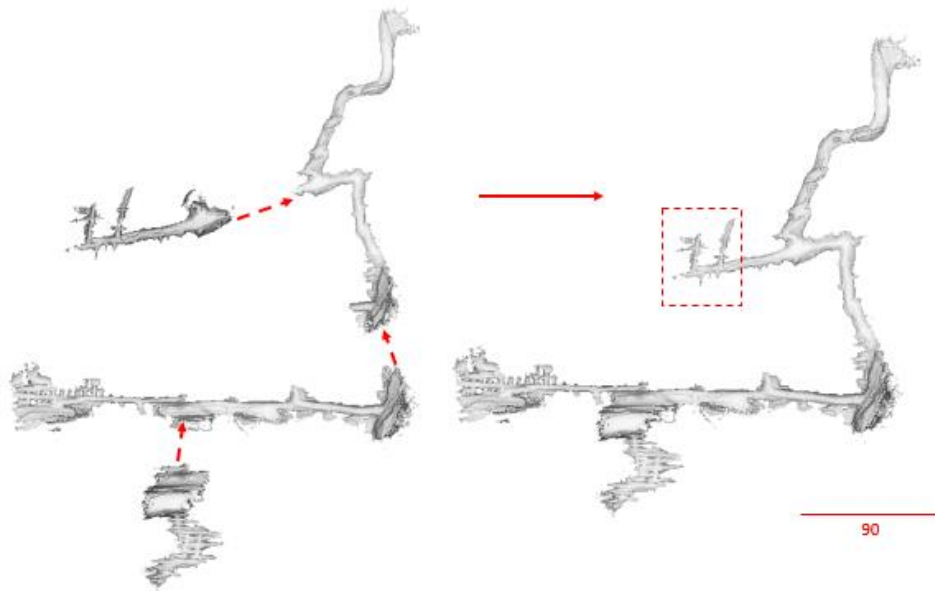


Figure 15-Point cloud alignment of TOR cave. Location in the box denotes the maze network with insufficient point density.

4.2 Geometry Analysis

4.2.1 Conduits Shape and Aspect Ratio

After investigating numerous cross sections of conduits in all five caves, the observed shapes can be generally categorized into five: horizontal ellipse, horizontal ellipse with notch edges, vertical ellipse, rectangular, and triangular shapes. Example cross sections of the different shapes are shown in table 5.

Table 5- Main conduit shapes observed in the geometry analysis of the caves.

Main Conduit Shapes Observed	
Horizontal Ellipse	
Horizontal Ellipse with Notch Edges	
Vertical Ellipse	
Rectangular	
Triangular	

Cross sections of the caves are taken at an incremental distance and aspect ratios are measured and plotted with distance. It is important to mention that in some caves few cross sections showed a rather flat base which is linked to the presence of sediment content at the floor of the cave. Not being able to predict the actual base of the tunnel is certainly a drawback towards accurately calculating the aspect ratio for some cave cross sections. Keeping that mind, certain values may be more precise than others. In other cross sections, aspect ratios were impossible to calculate due to difficulty in clearly delineating the boundary of a single tunnel or due to insufficient point density.

Gruta Diva De Maura:

Diva De Maura cave is located in the municipality of Seabra, state of Bahia. Cross sections are taken every 25 m distance (figure 16). In general, these show a dominant horizontal ellipse shape, with a flat base in the majority of them, denoting high presence of sediment content or dust from disaggregation at the floor of the cave.

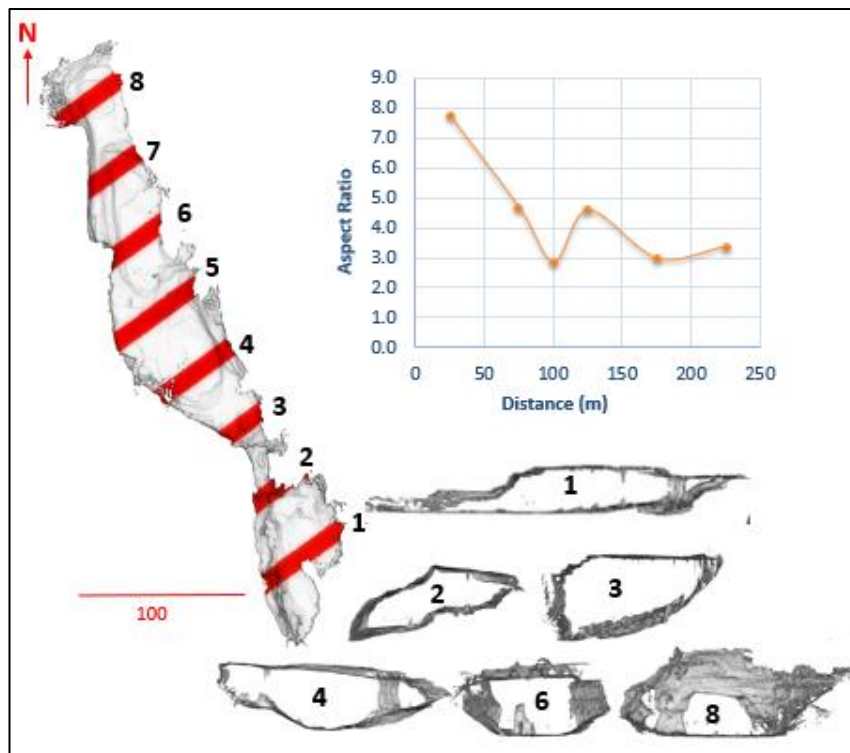


Figure 16-Cross sections and aspect ratio measurements with distance of DDM cave.

This cave records the highest aspect ratio among the studied caves (ranging between 2.85-7.73), due to its increased width which is influenced by the underground river coming from quartzite recharge area. As stated by (Audra, 2019), this cave's proximity to the Rio Preto river, which represents the regional base level, dictates its epigene origin and the influence it has on the evolution of its conduits.

Gruta do Ioiô:

The Ioiô Cave is located in the Patos Lagoon Village, in the municipality of Palmeiras, state of Bahia. Cross sections are also taken each 25 m of distance (figure 17). For cross sections 1 and 2 aspect ratio is difficult to compute as it shows there is a stacking of several tunnels above each other. In general, the shapes observed in this cave are also interpreted as horizontal ellipse with aspect ratios ranging from 1.59 to 3.27.

This cave is identified as a hypogene water table maze fed by deep rifts. It is thought to have recently been active or even still since rifts are not filled with sediments and certain morphologies are precisely associated to the present water table (Audra, 2019).

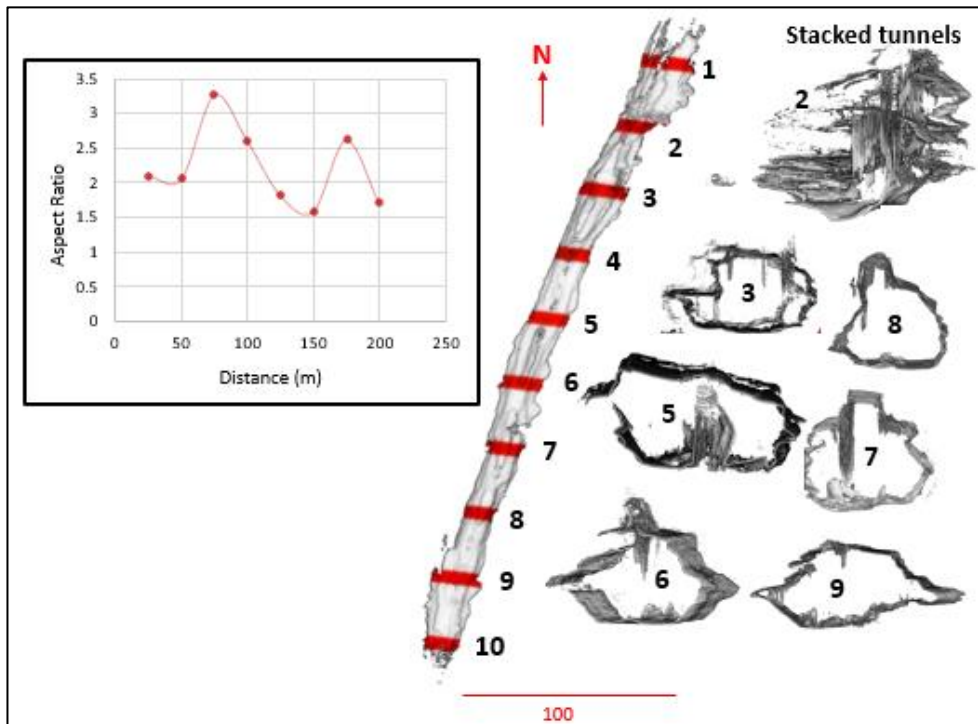


Figure 17- Cross sections and aspect ratio measurements with distance of IOI cave.

An obvious feature observed in cross sections of this cave is the presence of notch edges on the sides (cross sections 6,9). This is attributed to change in the water table whereby water rises from deep feeders and the notch position would correspond to the maximum enlargement at the water table (see figure 19, Audra 2019). The water table elevation then decreased (probably recently) because of drought and possible overexploitation of groundwater and therefore resulted in the V shaped walls that start at 12 m apart joining at a 2 m wide rift (Audra, 2019). Audra (2019) also states that as we move further away from the feeder, the rift gradually narrows till it reaches a dead end.

Hanif (2019) claims that the width of the cave passage decreases going from cross section 1 to 10 and therefore interprets the presence of a feeder near the location of cross section 1. However, according to the results of this study, maximum widths are observed at cross sections 6 and 9 and the width of the passage is seen to gradually decrease away from those locations (see figure 18). This suggests presence of two feeders at those two locations.

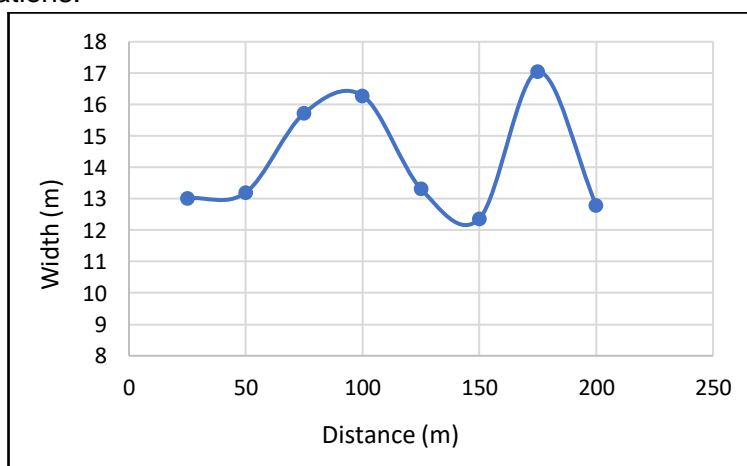


Figure 18-Change of width of IOI passage moving from cross section 3 till 10.

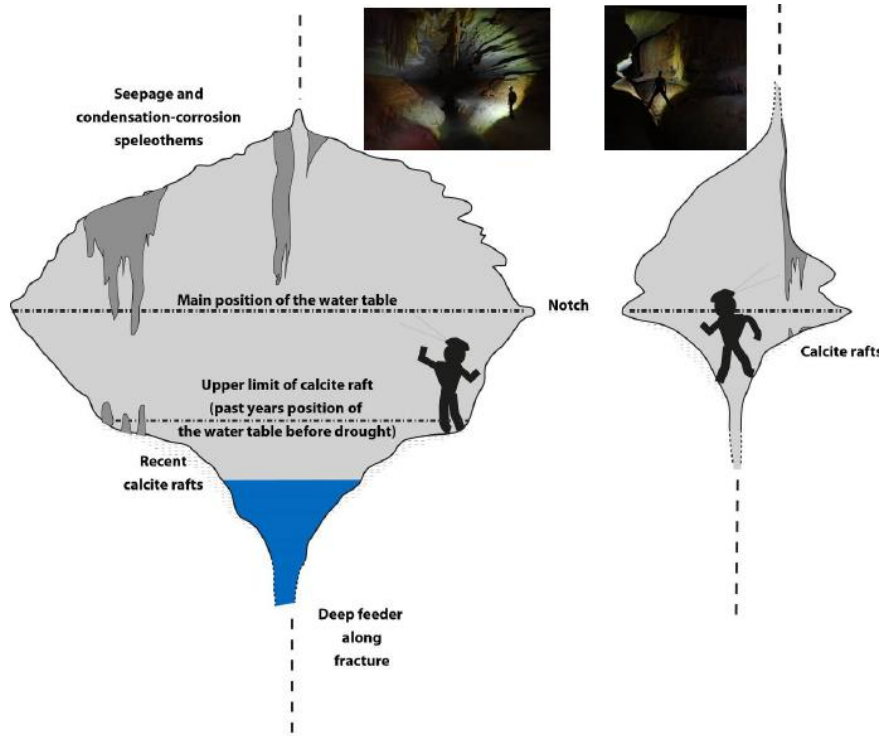


Figure 19-Illustration showing the geometry corresponding to changes in water table fed by deep rifts. Right diagram shows the rift gradually narrowing away from the feeder (Audra, 2019).

Gruta do Torrinha:

Torrinha is located in the municipality of Iraquara, in the state of Bahia and has 12 km long passageways. There is a clear distinction between the morphology of two parts of the cave (figure 20); part A shows a meandering pattern, and part B consists of mazes of rectilinear pattern. Both parts are investigated in detail through a number of cross sections.

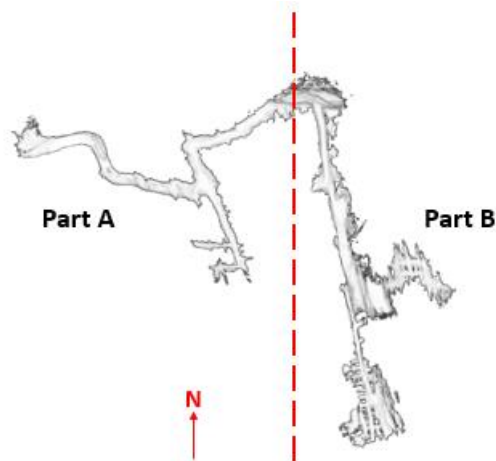


Figure 20-Boundary between two parts of the cave with different characteristics.

The meandering passageways of Part A are divided in 4 (as seen in figure 21). Cross sections in all parts show almost similar shapes classified as horizontal ellipse with aspect ratio values ranging between 1.72-4.40. A flat base is observed in several cross sections indicating presence of sediments at the base of the passageways.

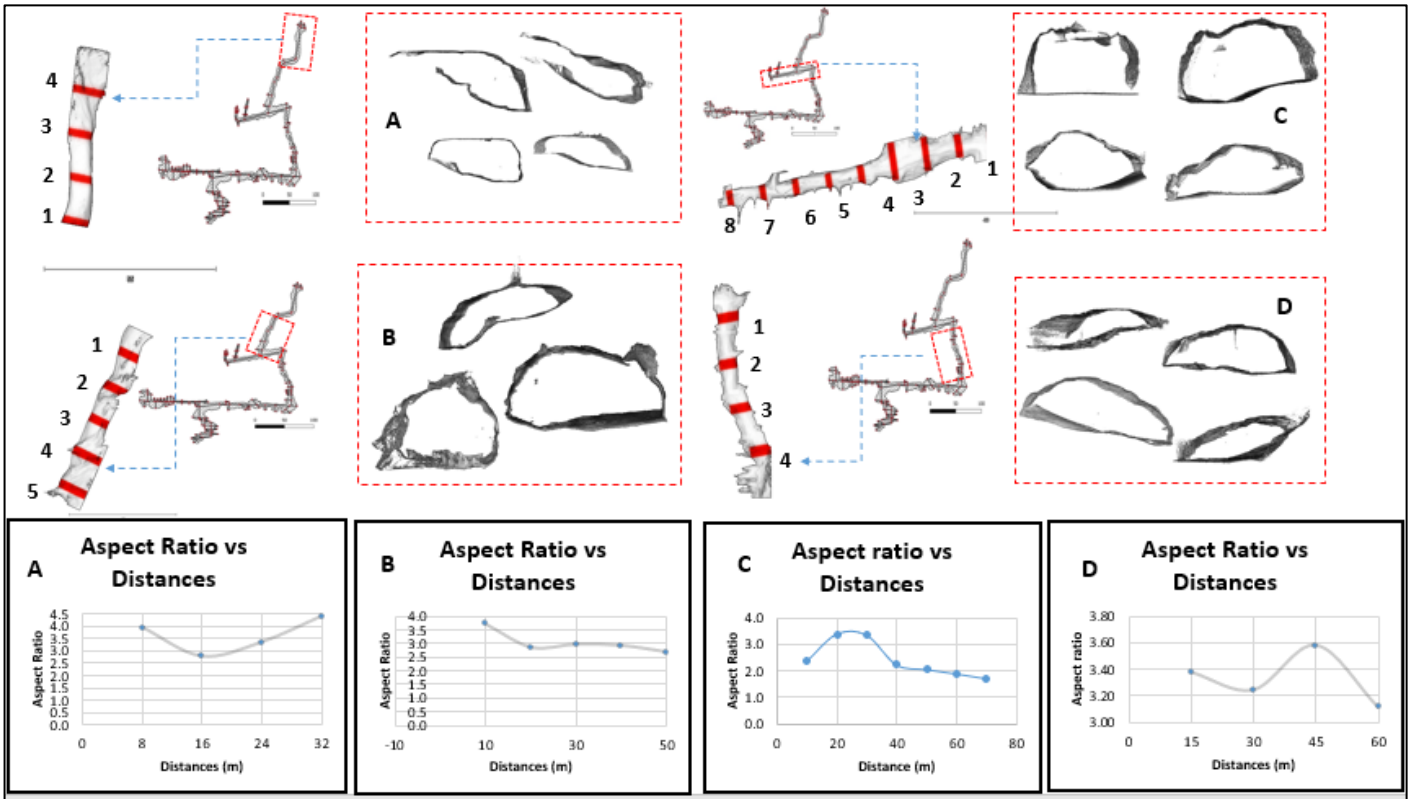


Figure 21- Cross sections and aspect ratio measurements with distance of *TOR-Part A*.

A distinct change is observed in Part B and where we no longer see any horizontal ellipse shape but a dominance of vertical ellipse shape. Cross sections of the main conduit are observed in figure. Aspect ratio values show almost a gradual increase going from cross section 1 to 12 with aspect ratios increasing from 0.39 to 0.81. Measurements on cross sections 7-9 are not made because the boundary is not clear.

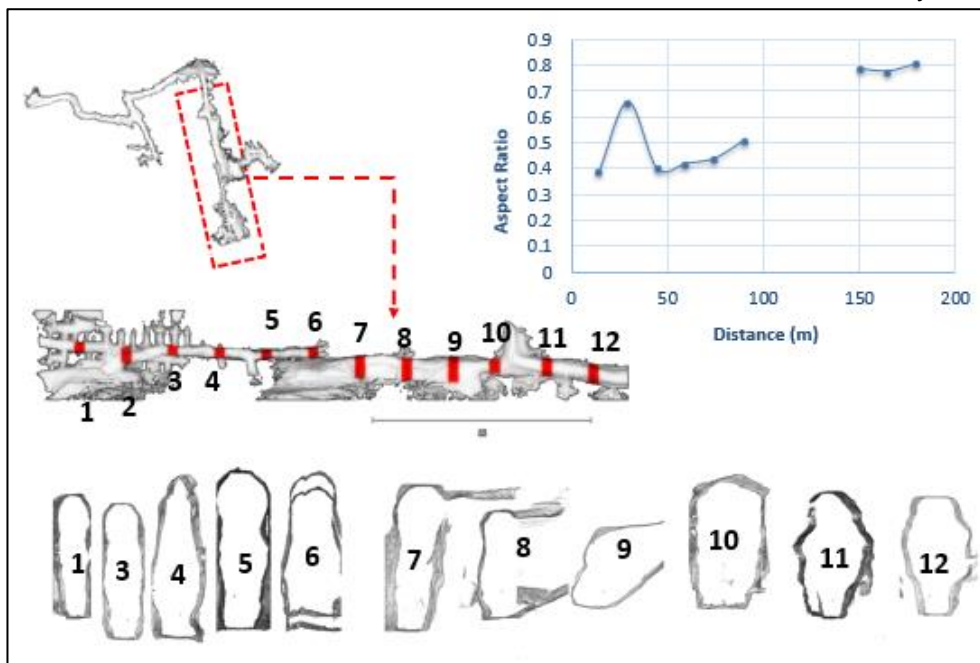


Figure 22- Cross sections and aspect ratio measurements with distance of *TOR-Part B*.

Part B consists of 2 mazes (figures 23, 24) with tunnels of aspect ratios below 1. No signs of lateral development of the conduits was observed at all in this part of the cave. Based on this analysis, it is clear that

there is a distinction in the geometry of the conduits besides just the geomorphological pattern of the two parts of *TOR* cave.

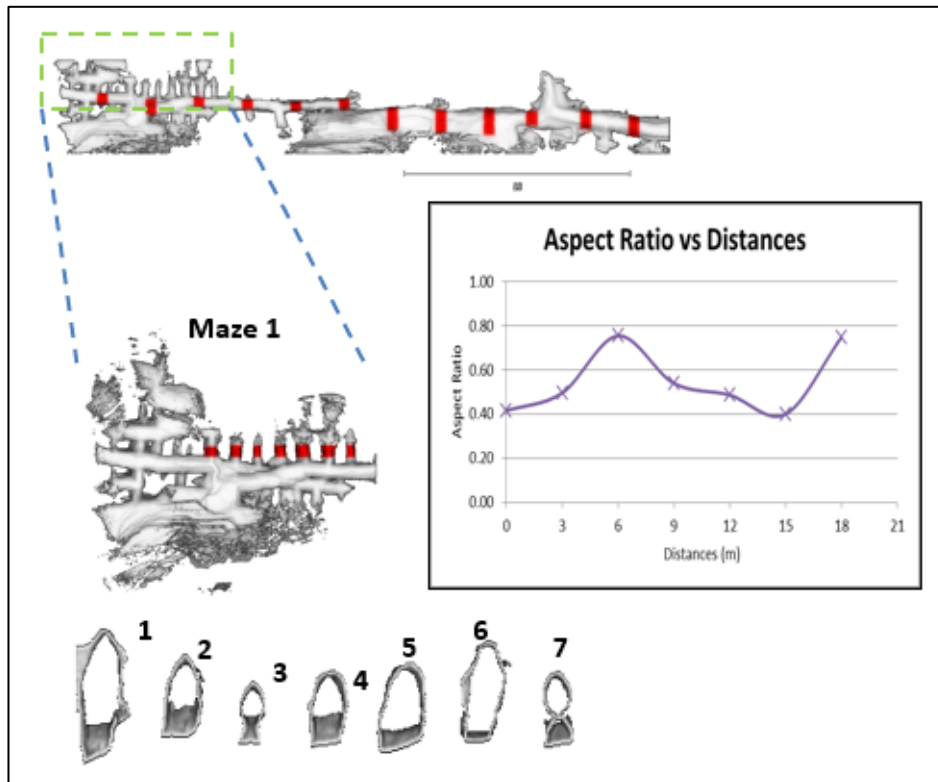


Figure 23- Cross sections and aspect ratio measurements with distance of *TOR*-Part B Maze 1.

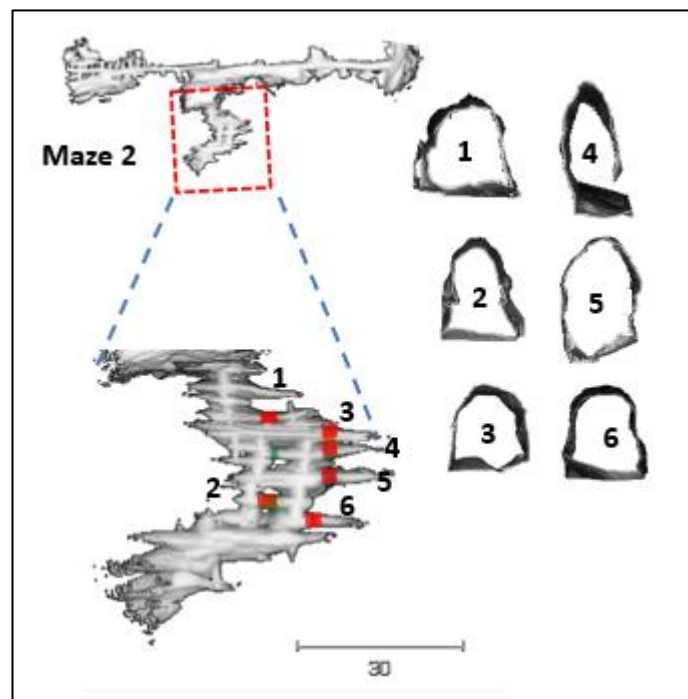


Figure 24- Cross sections of *TOR*-Part B Maze 2.

We might be able to speculate that both parts of the cave originate from a different system and thus giving this cave a mixed origin. Part A which resembles a meandering river system clearly displays its epigene origin and is as well stated by Audra (2019). The fact that we observe horizontal ellipse shape could be related to

the lateral process of dissolution that a fluvial system develops. On the contrary, in part B where only vertical ellipse geometries are observed, we could claim that this might be a result of hypogenic processes that has encouraged upward dissolution due to rising fluids and hence the vertical development of the conduits.

Audra (2019) believes that identifying the origin of those mazes is quite a challenge (they could be either hypogenic or floodwater maze) since possible early hypogene features have been obscured by later fluvial phase(s). Hanif (2019) claims presence of horizontal ellipse shapes in maze 2 linked to later phases of fluvial activity which brought in sediments and thus modified the shape. Based on the results of this study, no horizontal ellipse shapes of individual tunnels were observed at all in maze 2; the case those appear is when cross sections show 2 adjacent tunnels connected together and in fact not an individual tunnel.

Gruta da Lapinha:

The Lapinha cave is located in the municipality of Ibiquera, state of Bahia. This cave has a series of rectilinear conduits with large internal spaces that seem to have developed around a system of orthogonal fractures. The labyrinthine pattern indicate that it probably has an exclusive hypogenic origin (Audra, 2019). In terms of the conduits' shapes, the dominant shape is that of a horizontal ellipse with aspect ratios ranging 1.39-2.36. In some cases, it appears to be flat on top (cross section 1 & 2) which could be related to presence of silt layer on top.

The other shape which has appeared on some cross sections is the triangular shape. This has been observed in two cases:

1. Cross section 10: An accentuated roof due to the presence of an anticline which extends in the N-S direction. The base is covered with sediments and therefore appears to be flat. Resulting shape is a triangle.
2. Cross sections 3, 8, 9: Two thin conduits lying on top of each other but at some point become connected because of dissolution. The resulting shape appears to be a triangle attributed to a single conduit but in fact they are two separate conduits. This transition is observed clearer in cross section 9.

This cave appears to be inactive due to the presence of sediments at the base.

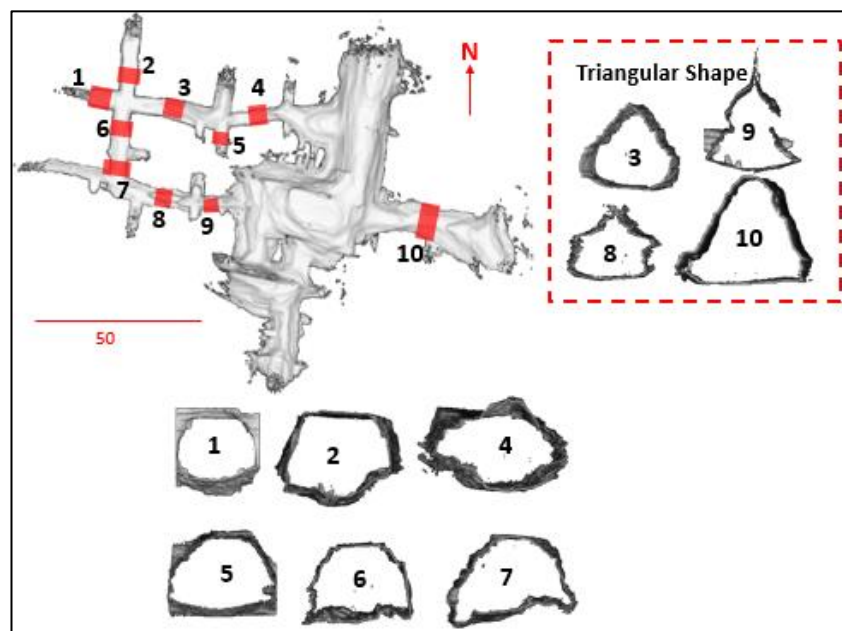


Figure 25- Cross sections of LAP cave.

Gruta da Paixão:

The Paixão Cave is located in the municipality of Andaraí, in the state of Bahia. Two shapes are observed from the cross sections of this cave: horizontal ellipse, and a more rectangular shape. Aspect ratios vary between 1.27 and 2.61. This cave is also identified as a hypogene water table maze and certainly an inactive one as we see a flat base in almost all of the cross sections.

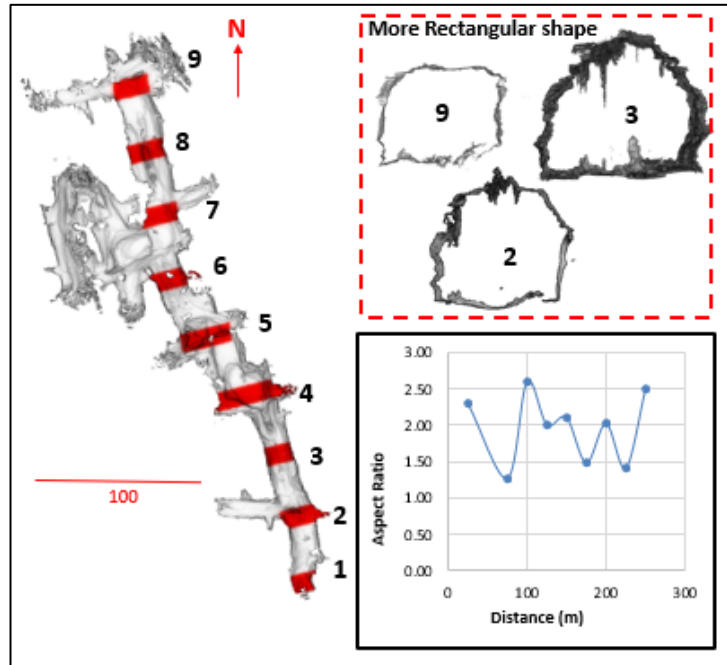


Figure 26- Cross sections and aspect ratio measurements with distance of PAX cave.

Two hypotheses could be formulated as to why we see a rectangular shape:

- First one is permeability related; when there is a soft impermeable (shale) layer on top of a strong permeable (fractured limestone) layer, the impermeable layer therefore acts as seal and stops fluid flow and the development of the conduit vertically.
- Second one is strength related; in cases of collapse.

4.2.2 Conduits Orientation

Gruta Diva De Maura:

Orientation analysis of the cave passage show in general two preferential orientations. Two caves are unidirectional: *DDM* (NNW-SSE), and *IOI* (NNE-SSW), while caves *PAX* and *LAP* conduits are developed in two orientations perpendicular to each other (N-S, E-W). Cave *PAX* shows a bit more scatter in orientations, however a dominant orientation is obvious in N-S. Results are shown in figures 27 to 31.

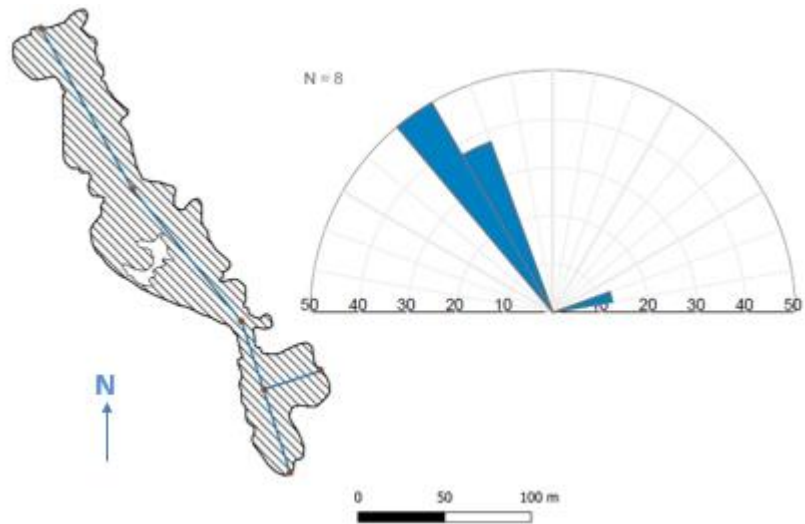


Figure 27-Orientation analysis of DDM cave showing a single preferential orientation.

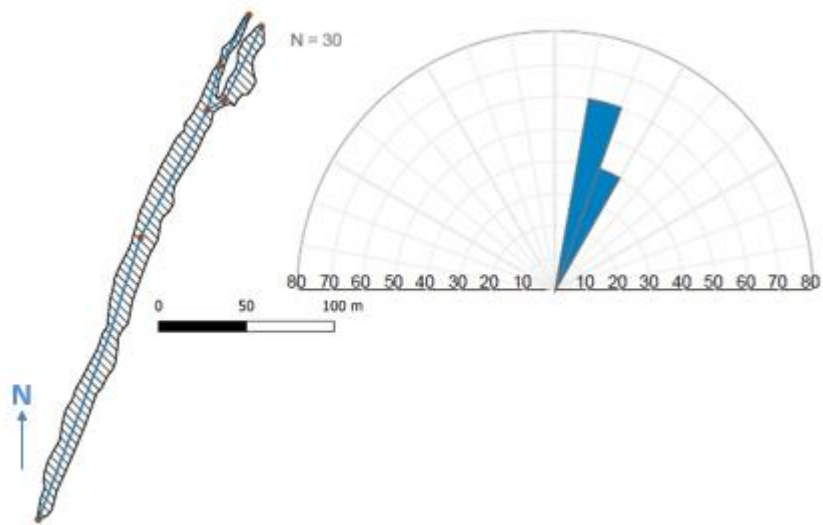


Figure 28-Orientation analysis of IOI cave showing a single preferential orientation.

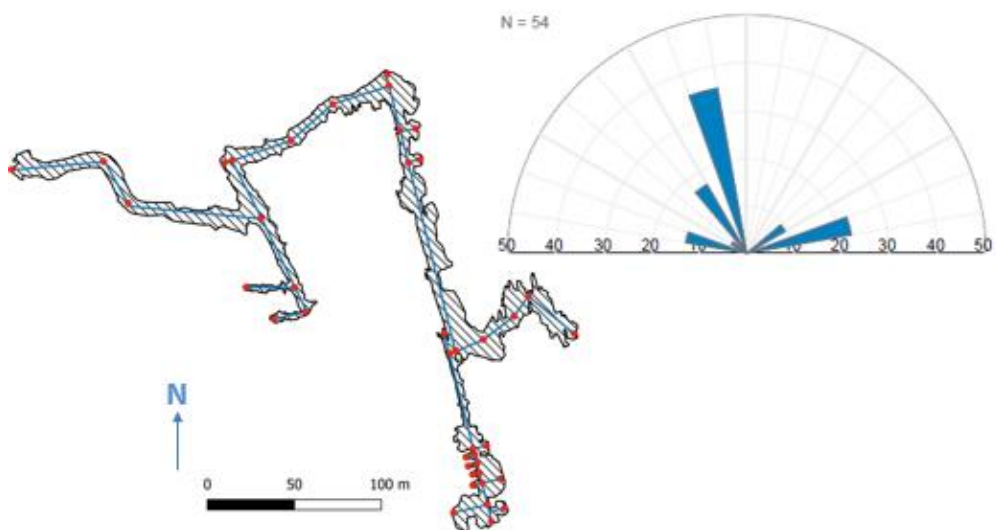


Figure 29-Orientation analysis of TOR cave showing two preferential orientations perpendicular to each other.

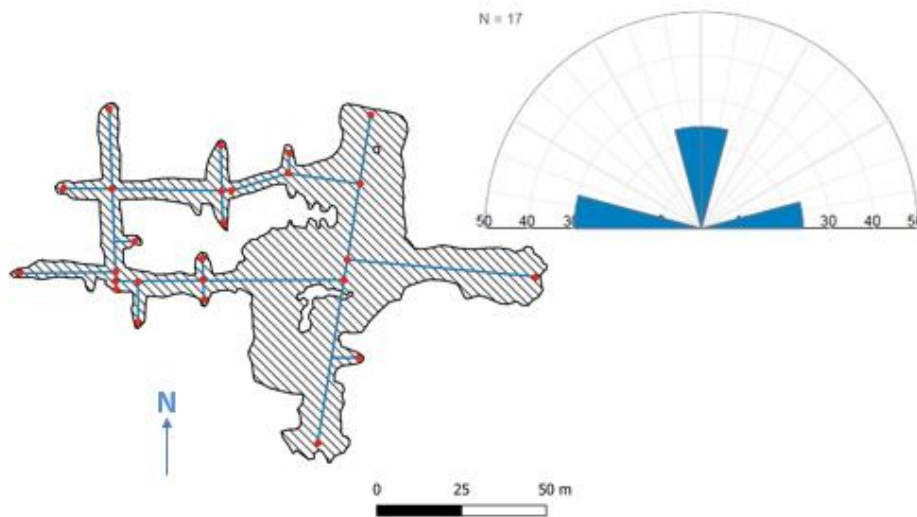


Figure 30- Orientation analysis of LAP showing two preferential orientations perpendicular to each other.

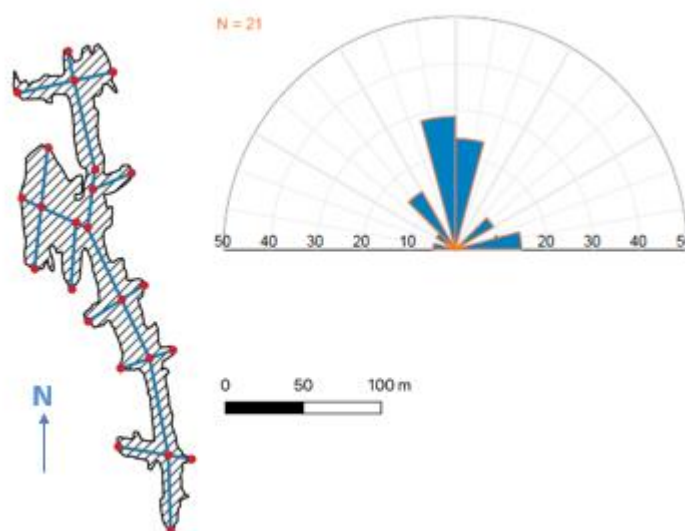


Figure 31- Orientation analysis of cave Paixao showing a dominant single orientation.

4.2.3 Discussion

Based on the geometry analysis, the main observed shapes can be in general classified into either a horizontal ellipse or vertical ellipse based on measurements of aspect ratios. Other modifications to the shape that were observed are related to certain processes occurring under the influence of factors like:

1. Changes in the hydraulic gradient where we see notches at the sides of the tunnel like in the example of loio cave (cross section 6).
2. Permeability, where presence of an impermeable layer on top of limestone could inhibit the vertical development of the tunnels and result in a rectangular shape with a flat ceiling as seen in Paixao cave (cross section 9).
3. Geological structures like in the case of the anticline present in Lapinha cave which yields a triangular form as a result (cross section 10). Influence of fractures is discussed in the following chapter.

There are certainly other factors that control the karstification process. Lowe and Gunn (1997) realized that some carbonate facies and bedding planes are favorable to karstification due to lithological or chemical

characteristics that further guide conduit development. They introduce the term “inception horizon” which describes “any lithostratigraphically controlled element of a carbonate sequence that passively or actively favors localized inception of dissolutional activity by virtue of physical, lithological, or chemical deviation from the predominant carbonate facies within the sequence” (Lowe & Gunn, 1997). This could explain why for example in Ioio and Lapinha caves we encounter a development of stacked conduits on top of each other which also at some point become connected as one due to varying dissolutional processes.

Regarding the distinction between conduits that are developed laterally in contrary to conduits developed in the vertical direction (Torrinha cave example), this may be related to the genetic origin of the system where the source and mechanism of fluid flow plays a role. In a hypogene system where karstification forms due to upwelling deep waters, presence of vertical ellipse shaped conduits could be evidence of the upward movement of fluid which differs fundamentally from surface-related epigene mechanisms. More evidence is needed to support this hypothesis and definitely we cannot rely only on the geometry of cave passages to understand the entire development process of the cave systems. Analysis of the shapes though can definitely confirm, in the case of Torrinha, that different underlying mechanisms took place and led to the distinct geometries of the tunnels.

4.3 Structural Analysis

The analysis of the structural data of all the caves indicated 3 main sets of fracture orientation: NNW-SSE (*DDM*), N-S (*TOR*), E-W (*LAP*, *PAX*), NNE-SSW (*PAX*, *LAP*) as seen in figure 32. Details of the structural data are found in appendix 4.

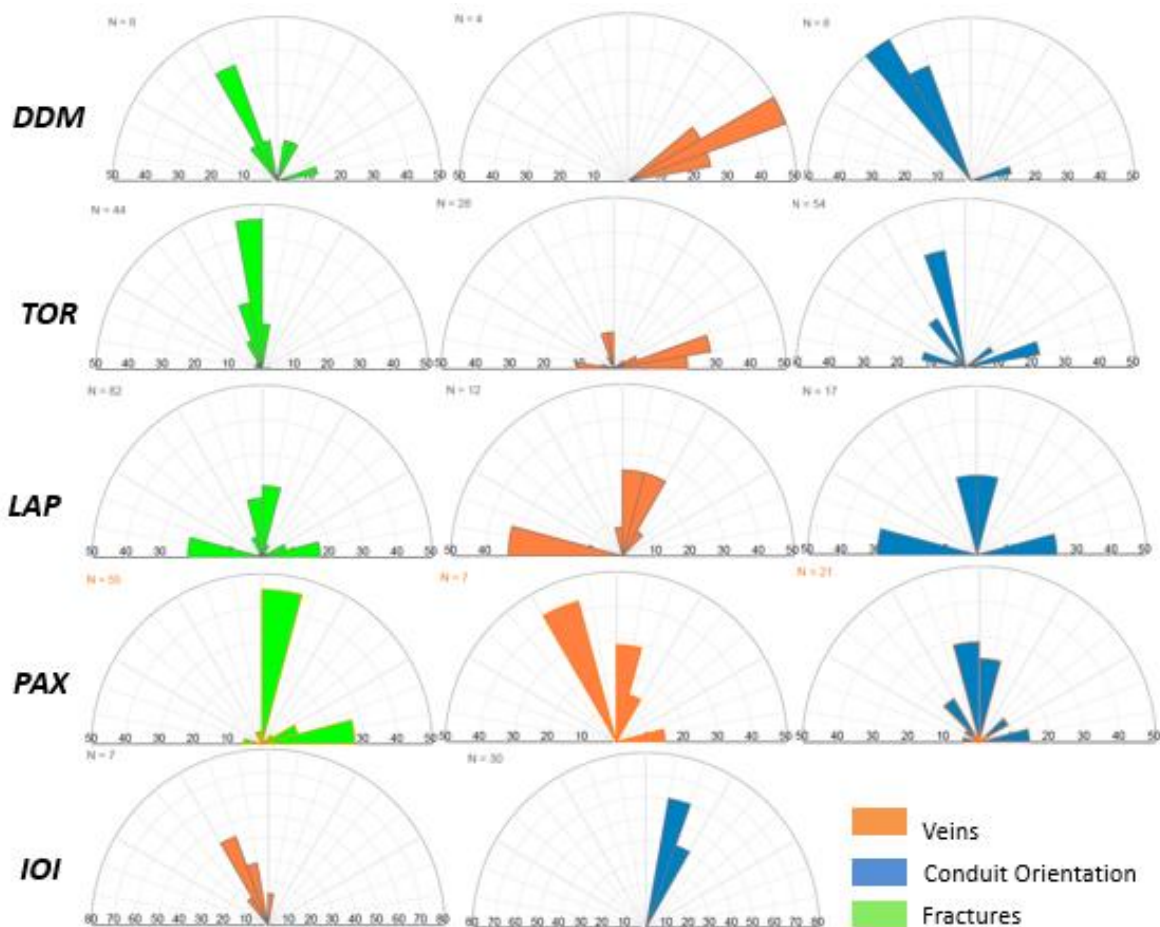


Figure 32-Rose diagrams showing orientations of fractures, veins and conduits in all of the caves.

Fractures have a major control on fluid flow and karstic development in carbonate rocks (Klimchouk & Ford, 2000). Primary porosity is usually very low in carbonates which is why secondary porosity plays a role in creating the path for fluid circulation. In a statistical study on the structural guidance of cave development, Palmer (1991) concluded that 42% of cave passages are controlled by fracture networks whereas only 1% were formed due to primary porosity. Klimchouk et. al (2009) investigated the relationship between fractures and speleogenesis and therefore divided fractures into three groups:

1. Pre-speleogenetic passive fractures, which are formed prior to speleogenesis and were hydraulically inactive during the period of speleogenesis due to very small aperture or complete infilling (veins).
2. Speleo-initiating fractures, which were hydraulically active during the period of speleogenesis and therefore guided the conduit development.
3. Post-speleogenetic fractures, which have formed at a later stage after speleogenesis, and indicated by offsets that are younger than the age of the cave passage.

Based on the results of the structural analysis, we can say that most of the fractures could be represented as speleo-initiating fractures as we see a correlation between the fractures and conduit orientation. It is therefore evident that the development and evolution of the conduits have been strongly influenced by fracture networks which almost certainly served as passages for fluid flow. Dominant vein orientations on the other hand do not show same correlation in some cases like in *DDM* and *IOI* which could possibly be identified as pre-speleogenetic passive fractures that had not been hydraulically active during the development of the cave passage due to the complete cementation.

Looking at the regional perspective, the karst patterns and the geologic structure correlate with the regional deformation of the Neoproterozoic units. The Neoproterozoic units have been influenced by two phases of deformation, NNE-SSW and E-W striking folds and thrusts, that resulted due to collisional events which occurred on the margin of the São Francisco Craton. This correlates with the dominant orientations of the fracture networks in the caves.

4.4 Stability Analysis

4.4.1 Numerical Simulation Results

Spalling criterion values are investigated in the areas surrounding the tunnels in order to identify the extent of the damaged zone. As mentioned earlier, values greater than 0.4 indicate initiation of fracturing and thus we would refer to this as the critical zone, whereby it is characterized by fractured or loosened rocks. Dimensions of the critical zone (see figure 33) are measured for the different tunnels and are shown in table 6. The severity of damage can be classified qualitatively as minor, moderate, and severe. Quantitatively, minor, moderate and severe damage would then be characterized by critical zones less than 0.25m, 0.25-0.75m, and greater than 0.75m respectively (Kaiser et.al, 1996). At the depth of 500m all tunnels except for slice 2 show two critical zones on each side of the tunnel. Tunnel 2 has no fracturing at all at this depth. Tunnels 1, 4, and 5 all indicate severe damage while tunnel 3 indicates moderate damage.

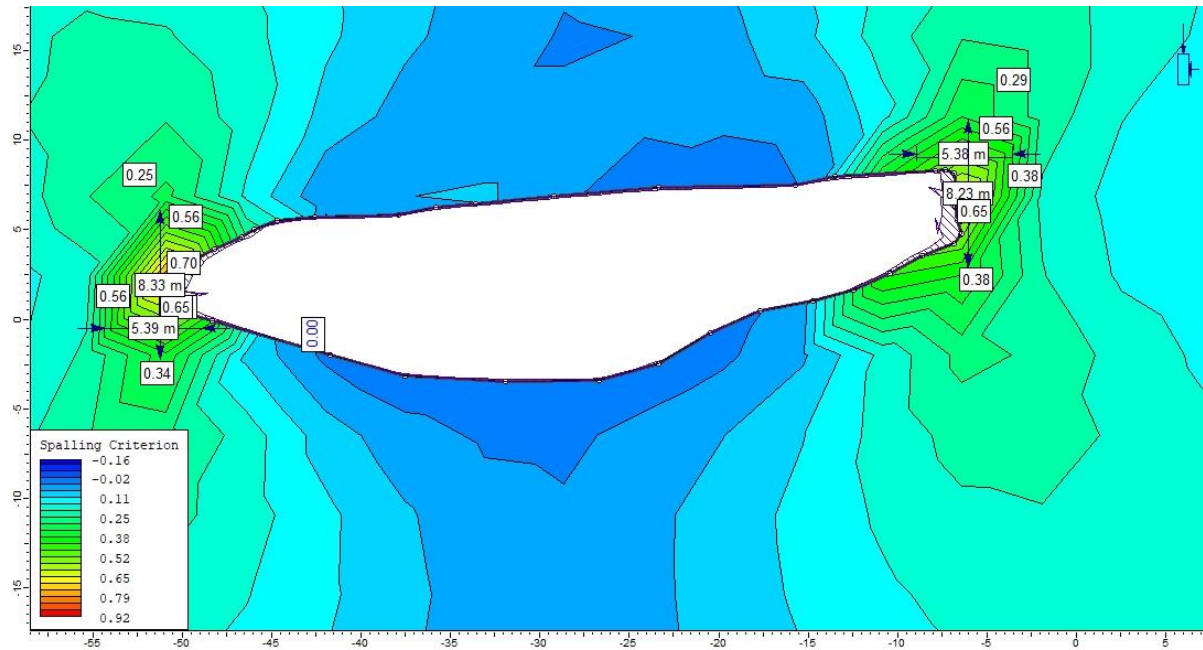


Figure 33-Contour plot of spalling criterion values for tunnel 1 showing how width and height of the critical zone are measured based on spalling values greater than 4.

Table 6-Critical zone dimensions for the different tunnel slices at a depth of 500m.

Cave	Slice Number	Critical Zone Dimensions	
		Width	Height
DDM	1	5.39 & 5.38	8.33 & 8.23
TOR	2	0	0
LAP	3	0.31 & 0.66	0.93 & 0.55
IOI	4	2.30 & 0.92	2.40 & 2.37
PAX	5	1.12 & 0.56	1.32 & 1.47

Figure 34 shows how far from the tunnel boundary deformation has taken place with increasing depth. Deformation for tunnel 1 starts the first which is at a depth of 300 m, it increases gradually and reaches 25 m distance away from the tunnel at a depth of 1700m. Critical zones for tunnels 4 and 5 start at depth 400 m and extend about same distance from the tunnels boundary except that for tunnel 4 it does at a later depth. Deformation around tunnel 3 extends very little gradually with depth and reaches only around 4 m at the depth of 1700m. Deformation for tunnel 2 starts the latest, at a depth of 800m, and extends a few meters away from the tunnel boundary.

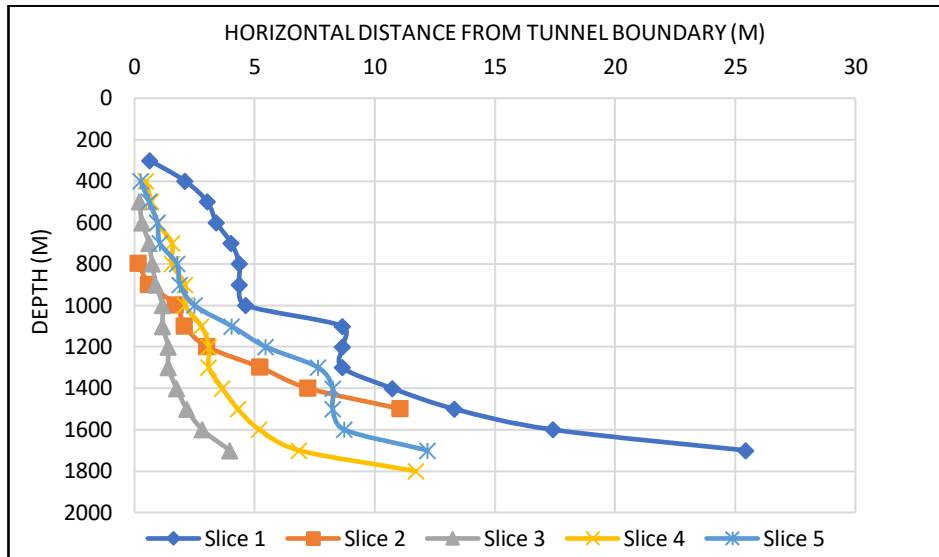


Figure 34-Width of deformed zones horizontally from the tunnel boundary with depth for the different tunnels.

Collapse potential is also investigated based on the Spalling Criterion values that reach 7 and higher in the region surrounding the tunnel. The depth at which we start to see those values exceeding the threshold of 7 in the critical zone could imply collapse potential. This is considered the minimum depth of collapse potential; results are shown in table 7. In terms of comparing the stability of the different shapes, we can definitely conclude that tunnels of horizontal ellipse shape have far less stability than the vertical ones. For an aspect ratio of 3.2, minimum depth of collapse potential is 500 m while for a tunnel with an aspect ratio of 0.4 it is 1150 m. Figure 8 shows how maximum shear strain increases with increasing aspect ratio and therefore, we would expect less stability the higher the aspect ratio.

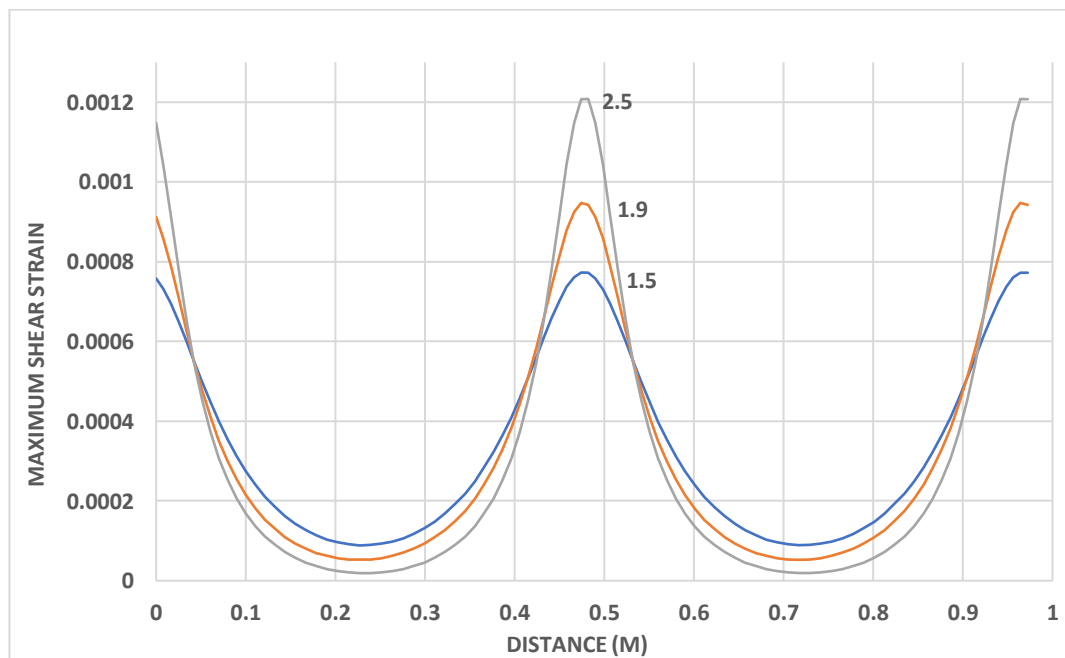


Figure 35-Comparison of maximum shear strain values for tunnels with different aspect ratios.

The dimension of the tunnel is tested for the effect on the stability in comparison to the aspect ratio parameter. Two experiments were performed, the first one includes keeping the aspect ratio constant while changing the

dimension of the tunnel, and the second one includes changing the aspect ratio while keeping the dimension constant. Results show that change in the aspect ratio causes a significant change in the stability, while changing the dimension had a little effect (see figure 36, note that there are two x-axes, top one referring to tunnel dimension and bottom one referring to aspect ratio).

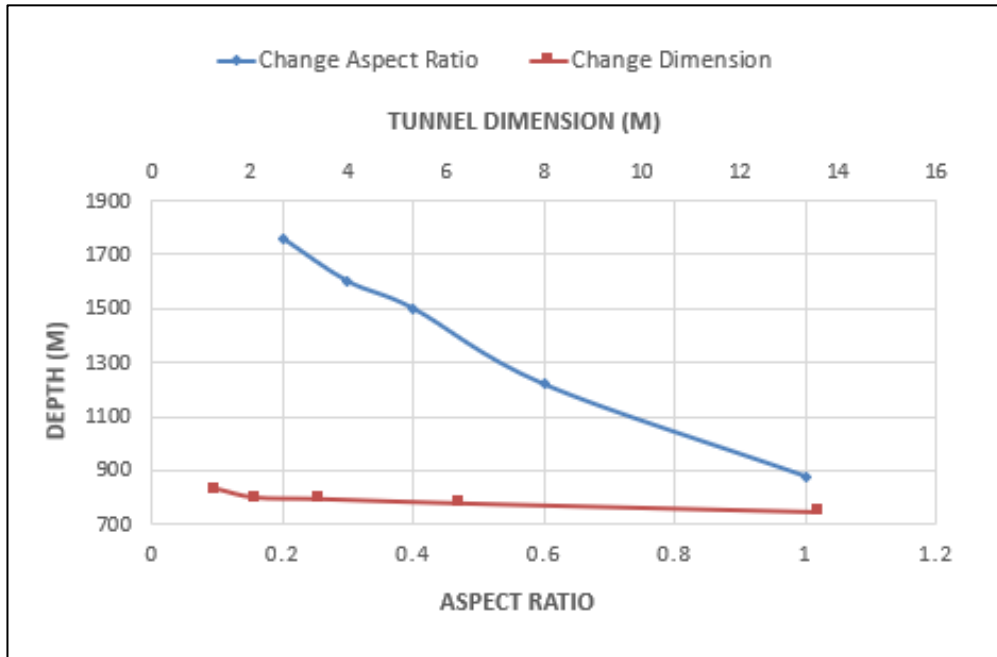


Figure 36- Plot showing the effect of changes in tunnel dimension compared to changes in the aspect ratio. Note that there are two x-axes in the plot, the top refers to tunnel dimension and the bottom one refers to the aspect ratio.

Table 7-Minimum depth of collapse potential for the different tunnel slices.

<i>Cave</i>	<i>Slice</i>	<i>Minimum depth of collapse potential (m)</i>
<i>DDM</i>	Slice 1	500
<i>TOR</i>	Slice 2	1150
<i>LAP</i>	Slice 3	560
<i>IOI</i>	Slice 4	530
<i>PAX</i>	Slice 5	600

Minimum depth of collapse potential for the all the studied tunnel geometries are plotted against the aspect ratio in figure 37. As expected, the tunnel with the highest aspect ratio 4.3 has the least stability while the tunnel with the lowest aspect ratio 0.4 has the highest stability among the tunnel geometries. What is unexpected is the difference in stability between tunnels 3 and 5 which have the same aspect ratio of 1.4 but one has an angular form resembling more of a rectangle than an ellipse. One would think that presence of sharp edges, like in the case of a rectangle, would drastically affect the stability as these could be zones of weakness due to the high stress localization at those points, however the result shows that the angular form has a higher stability.

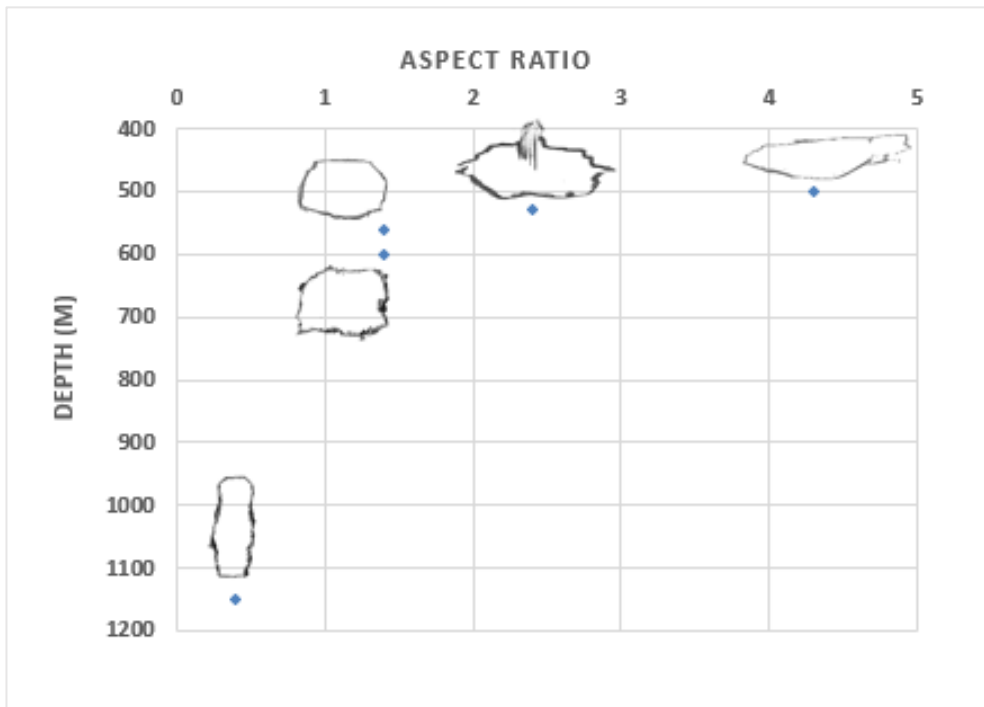


Figure 37-Estimated minimum depth of collapse potential for the different tunnel geometries with respect to aspect ratio.

A simulation model is performed on a set of ellipses and rectangles to check for resulting stability difference between the two shapes, taking into account the aspect ratio (figure 38). It did show that for rectangles with aspect ratios less than and greater than 1, the stability is higher than the counterpart ellipse shape of same aspect ratio. Though such a result is unexpected, similar result has been found in another study done by Wilson et. al, 2014 on tall rectangular tunnels versus arched tunnels. Wilson defined stability with reference to internal tunnel pressures. As such, with increasing overburden the total force resisting failure would then be proportional to the perimeter of the tunnel. Since an elliptical tunnel has a smaller perimeter than a rectangular tunnel, Wilson states that it would be reasonable to surmise that larger internal tunnel pressures would be required to resist the loads driving collapse. Results of the present study show that this could be the case except for when the aspect ratio is equal to 1. More research is required to prove this hypothesis and reasons behind it.

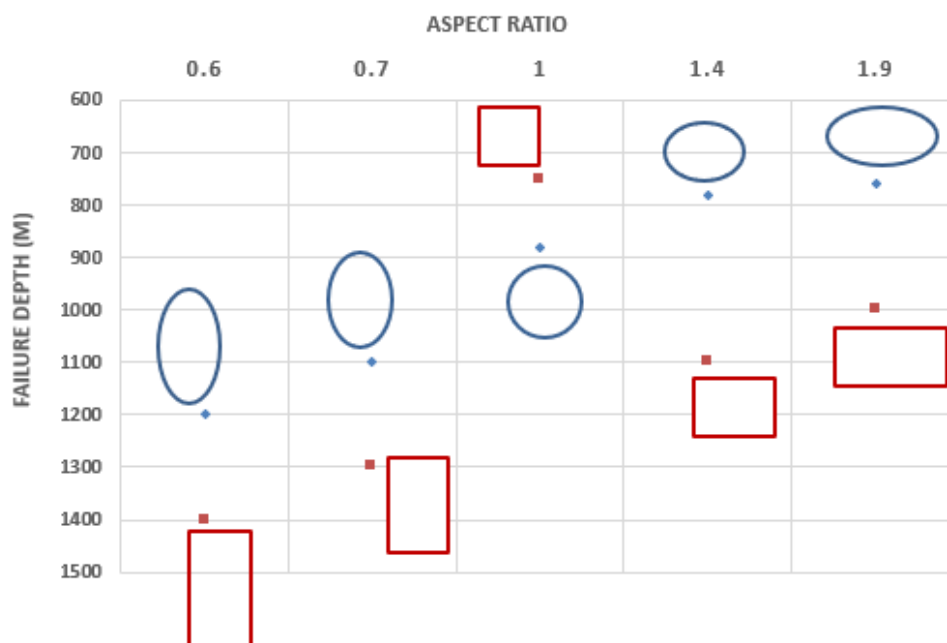


Figure 38-Comparison between a rectangular and ellipse geometry stability for different aspect ratios.

4.4.2 Sensitivity of parameters

Sensitivity analysis is carried on a cross section of one of the tunnels in order to check which input parameters have the highest effect on the results of the simulation model. In terms of the rock mass strength parameters, cohesion had the highest effect, friction angle had a slight effect, and tensile strength had no effect at all. Overburden unit weight sensitivity test also shows higher values of deformation with the increasing overburden.

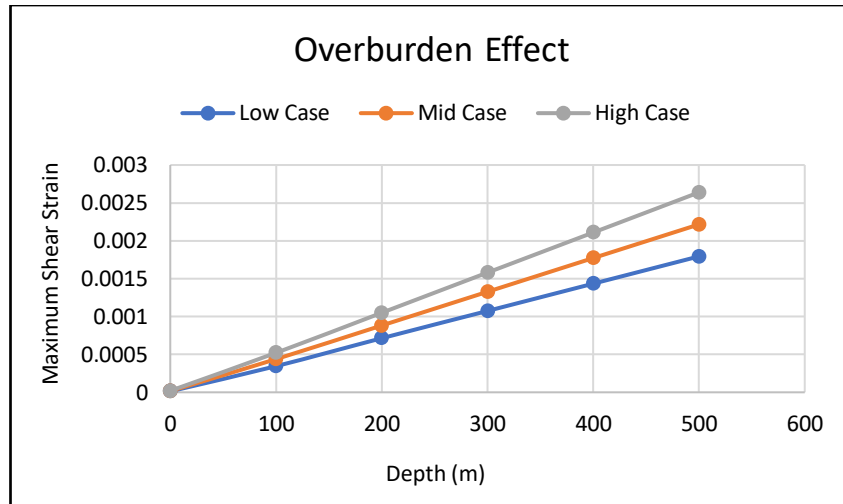


Figure 39- Sensitivity analysis of overburden.

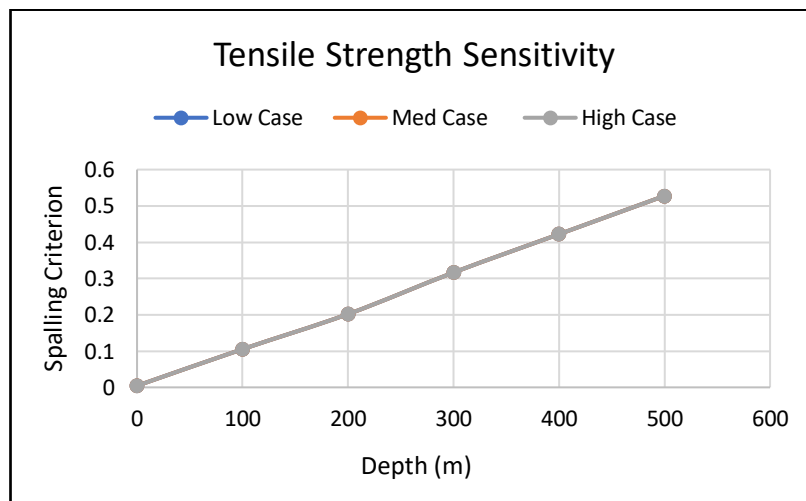


Figure 40- Sensitivity analysis of tensile strength.

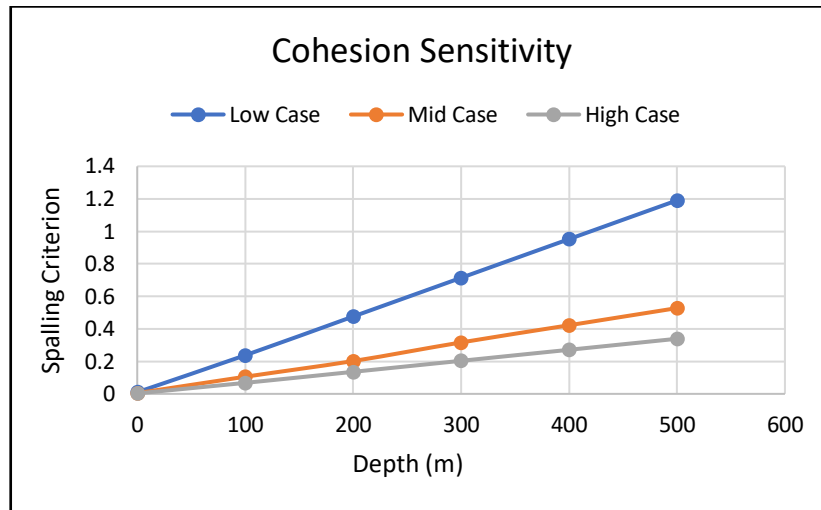


Figure 41- Sensitivity analysis of cohesion.

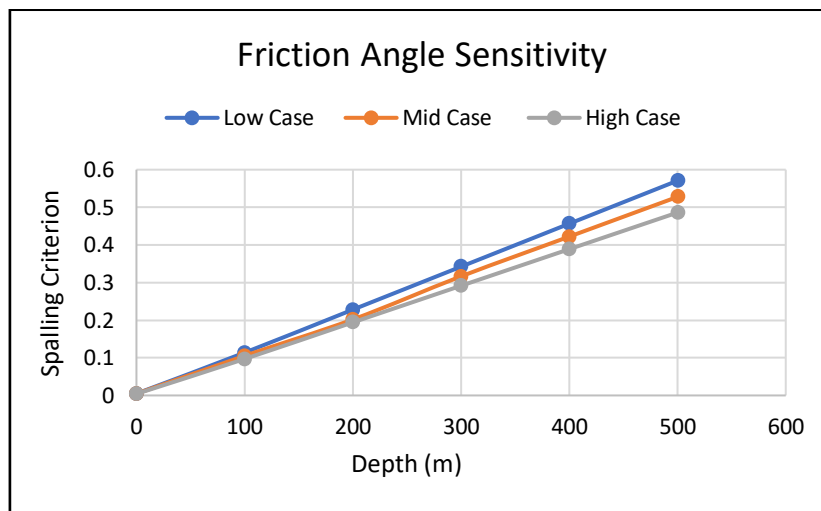


Figure 42- Sensitivity analysis of friction angle.

4.4.3 Discussion

It is of high importance to study if the rock surrounding the cave is overstrained or has undergone severe deformation because then we could map out areas of cave systems where collapse is possible to happen and the extent of the damaged zone. At surface elevation all caves are well stable and breakouts are very unlikely to happen. If we try and imagine such systems at reservoir depths then we would expect, according to results of the present model, that all caves would have somehow collapsed. In fact, seismic data from an area in the Campos Basin SE Brazil has shown numerous closed circular depressions which were interpreted as collapse sinkholes linked to supra- and intrastratal deformation (Basso, 2018). For this present study, almost all tunnels with a horizontal ellipse geometry are supported with rock that is already undergoing severe deformation at a depth of 500m. As far as the exact depths of collapse potential, there is definitely an uncertainty to that keeping in mind that this software only calculates elastic deformation which may be a small part of the actual deformation that occurs in the field. The model also assumes a void tunnel which also eliminates the effect of fluid pressure which in reality is not the case. Adding to that, if rock properties specific to each of the caves are available then results would also be more reliable. In some cases, as well, systems tend to collapse as a whole when exposed to overburden stresses generating coalesced collapsed paleocave (Loucks, 2007). Therefore, we would expect that interconnectivity between caves and tunnels also plays an important role in the geomechanical stability and prediction of collapse which should also be taken into account and investigated more.

This geomechanical analysis still provides quite useful information on behavioral trends of stress and strain for various tunnel geometries and can be improved with more research.

Conclusion

5.1 Conclusion

Several studies have shown the importance of karst network geometry and structure for understanding flow mechanisms. The fact that carbonate reservoirs host a high percentage of the world's hydrocarbon reserves invites many researchers and practitioners into understanding the distribution of karst network. In many cases, the network geometry remains unknown due to poor 3D seismic resolution. This research provides a study of accessible cave systems which can be considered as direct analogues to subsurface karst networks. Using 3D LIDAR surveys, the internal geometries are observed and analysed through metrics including measurements of aspect ratios and passage orientations while linking observations to possible underlying speleogenetic processes.

In general, two main shapes of tunnels are observed, horizontal ellipse and vertical ellipse shapes based on the measurements of aspect ratios. Several factors come in to play controlling the karstification processes and the resulting differences in geometry. In most cases the development of the cave systems was seen to be related to inception features like fracture networks and possible lithology contrast. Analysis of the conduit orientations in general shows two existing preferential orientations for the development of the cave passages, N-S and E-W. Correlation with field structural data indicated a structural control which aligns with the regional phases of deformation corresponding to collisional events that occurred on the margin of the São Francisco Craton.

Stability analysis of the tunnel geometries shows that tunnels with vertical ellipse shape have much higher stability than tunnels with horizontal ellipse shape. Results of the present study show that almost all tunnels with a horizontal ellipse geometry are supported with rock that is already undergoing severe deformation at a depth of 500m. The aspect ratio was found to be a major parameter controlling the stability of the tunnels, on the contrary the dimension of the tunnel showed a much less effect. Under the set of input parameters that was used in the present numerical model, a tunnel with rectangular shape showed higher stability than an ellipse shape. Possible explanation was discussed however more research is needed to confirm this hypothesis. Sensitivity test showed that overburden and rock mass strength parameters including cohesion and friction angle have the highest effect on the stability results.

5.2 Recommendations

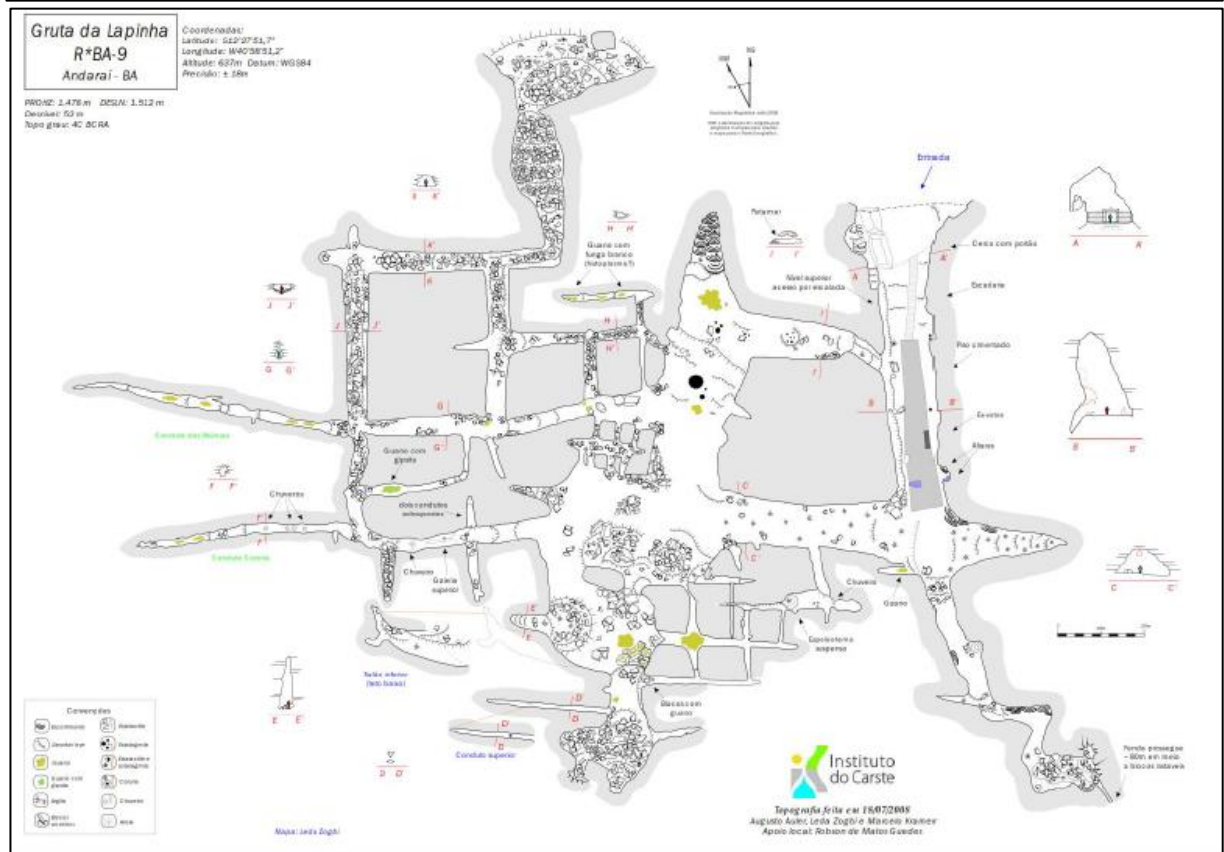
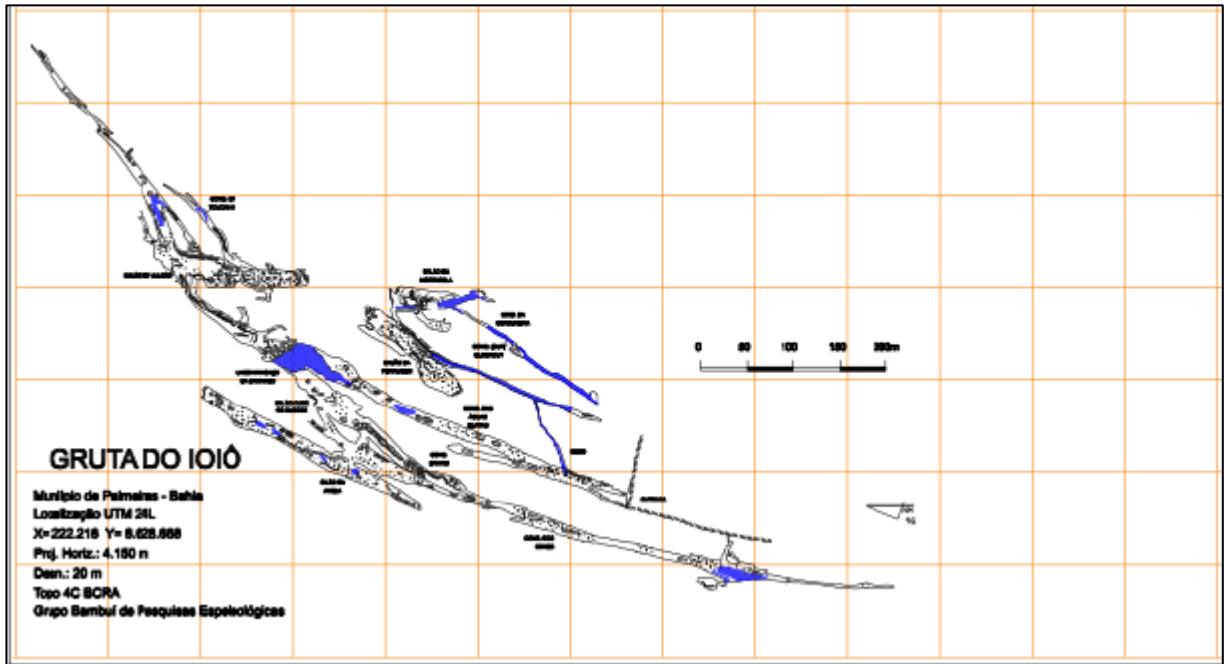
Most of the methodologies developed in this project were performed manually. For future, more investigation into developing certain algorithms for point clouds processing could maybe help automatically extract more metrics for characterizing the network geometries. Subsurface data acquisition would be helpful to determine the real base of the tunnels since in many of the caves, the floor appeared to be covered with sediments. Such data could be used to improve the measurement results of this research. Interpretations of the underlying speleogenetic processes and the origin of the cave systems can be certainly improved by integrating more field-based investigations including geochemical analysis of rock samples.

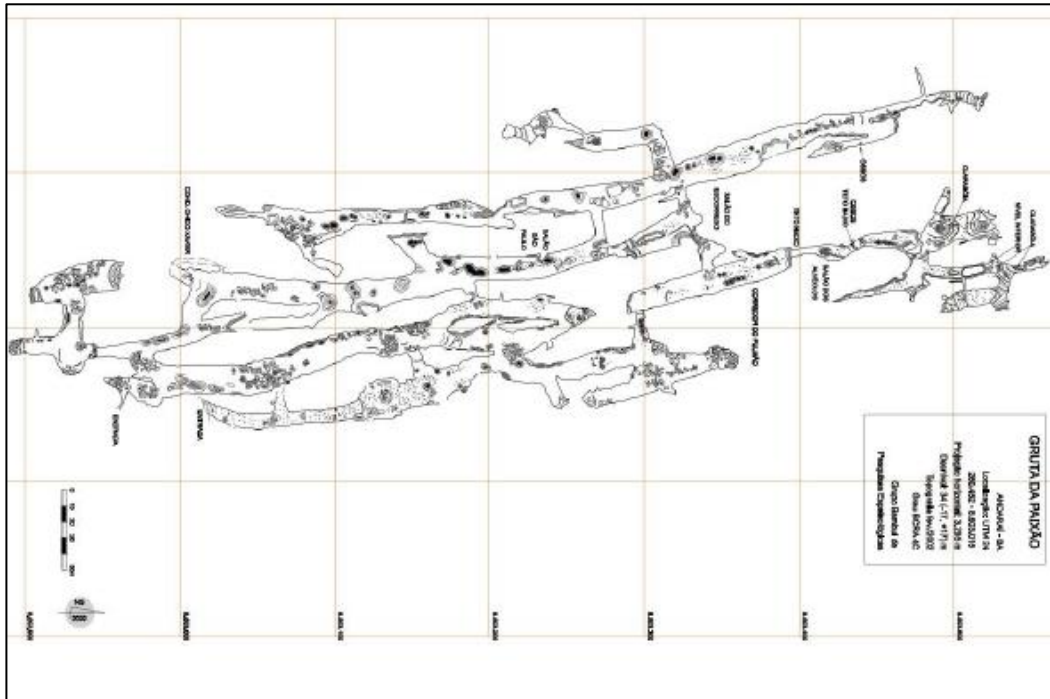
The boundary element method (*BEM*) used for the stability analysis is based on a mesh of the boundary only, therefore use of alternative numerical techniques like the finite element modelling (*FEM*) which discretizes the entire rock mass could help improve the results taking into account the cavity infill and pore pressure. Last, collecting rock properties that are specific to the lithologies in each of the caves would help improve the stability model.

Bibliography

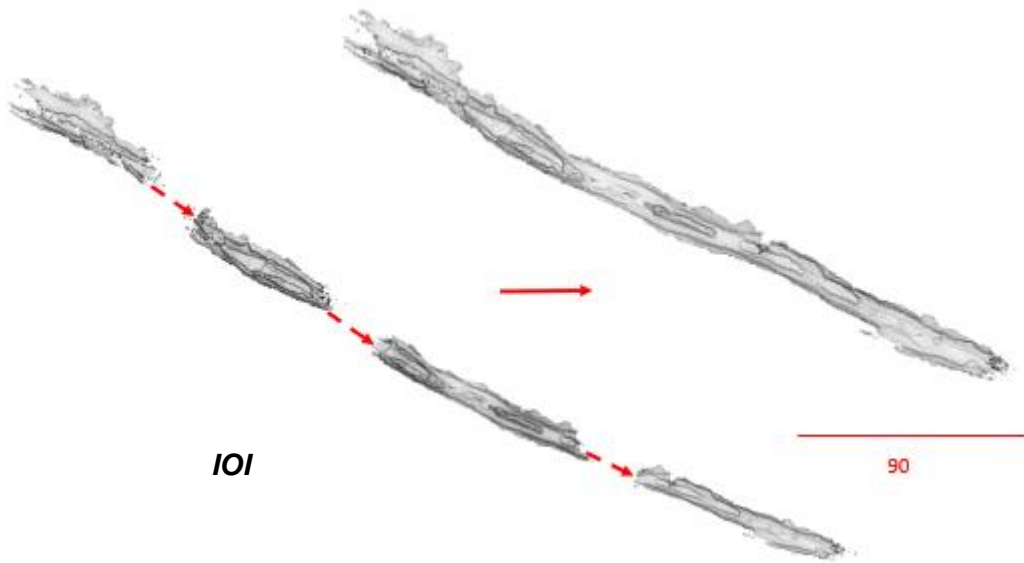
- [1] Auler, Augusto. (2002). Karst areas in Brazil and the potential for major caves - an overview. *Boletín de la Sociedad Venezolana de Espeleología*. 36. 29-35.
- [2] Auler, Augusto & Farrant, Andrew. (1996). A brief introduction to karst and caves in Brazil. *Proceedings of the University of Bristol Speleological Society*. 2. 187-200.
- [3] Audra P, Hobléa F, Bigot JY, Nobécourt JC (2007). The role of condensation-corrosion in thermal speleogenesis. Study of a hypogenic sulfidic cave in Aix-les-Bains. *Acta Carsologica* 36:185–194.
- [4] Audra P., Waele J. De, Pisani L., Del U. (2019). Processes and properties in fractured and karstified carbonate reservoirs.
- [5] Audra P, Mocochain L, Bigot JY, Nobécourt JC (2009b) Hypogene cave patterns. In: Klimchouk AB, Ford DC (eds) *Hypogene speleogenesis and karst hydrogeology of Artesian basins*. Special Paper, Ukrainian Institute of Speleology and Karstology, Kiev, vol 1, pp 17–22.
- [6] Audra P, Mocochain L, Bigot JY, Nobecourt JC (2009c) The association between bubble trails and folia: a morphological and sedimentary indicator of hypogenic speleogenesis by degassing, example from Adaouste Cave (Provence, France). *Int J Speleol* 38(2):93–102
- [7] Audra P., 2017 – Hypogene caves in France. In: Klimchouk A., Palmer A.N., De Waele J., Auler A.S. & Audra P. (Eds.), *Hypogene karst regions and caves of the world*. Springer, Cham, p. 61-83.
- [8] Basso M., Kuroda M. C., Afonso L. C. S., Vidal A. C. 2018. Three-Dimensional Seismic Geomorphology Of Paleokarst in the Cretaceous Macae Group Carbonates, Campos Basin, Brazil. *Journal of Petroleum Geology*, Vol. 41(4), pp 513-526.
- [9] Collon, P., Bernasconi, D., Vuilleumier, C., & Renard, P. (2017). Statistical metrics for the characterization of karst network geometry and topology. *Geomorphology*, 283, 122-142.
- [10] Diederichs M.S., Carter T., Martin D., 2010. *Practical Rock Spall Prediction in Tunnels*
- [11] Ennes-Silva, A., Francisco H.R. Bezerra, Francisco C.C. Nogueira, Fabrizio Balsamo, Alexander Klimchouk, Caroline L. Cazarin, Augusto S. Auler, Superposed folding and associated fracturing influence hypogene karst development in Neoproterozoic carbonates, São Francisco Craton, Brazil, *Tectonophysics*, Volume 666, 2016, Pages 244-259.
- [12] Esterhuizen, G.S., Dolinar, D.R., Ellenberger, J.L., Prosser, L.J., Iannacchione, A.T., 2007. Roof stability issues in underground limestone mines in the United States. In: Peng, S.S., Mark, C., Finfinger, G., Tadolini, S., Khair, A.W., Heasley, K., Luo, Y. (Eds.), *Proceedings of the 26th International Conference of Ground Control in Mining*. West Virginia University, Morgantown, WV, pp. 336–343.
- [13] Goodman, 1989. *Introduction to rock mechanics*, 2nd edition.
- [14] Hamdan N., 2013. *Two-Dimensional Numerical Modelling of Wave Propagation in Soil Media*.
- [15] Hoop, S. De, & Prabhakaran, R. (2018). Report Molengraaff Fund Grant 3D Outcrop Study of Hypogene Karst Caves of Brazil using LIDAR and Drone Imagery.
- [16] Islam H., 2019. *Geomtery and Stability Analysis of Caves in Bahia, Brazil*.

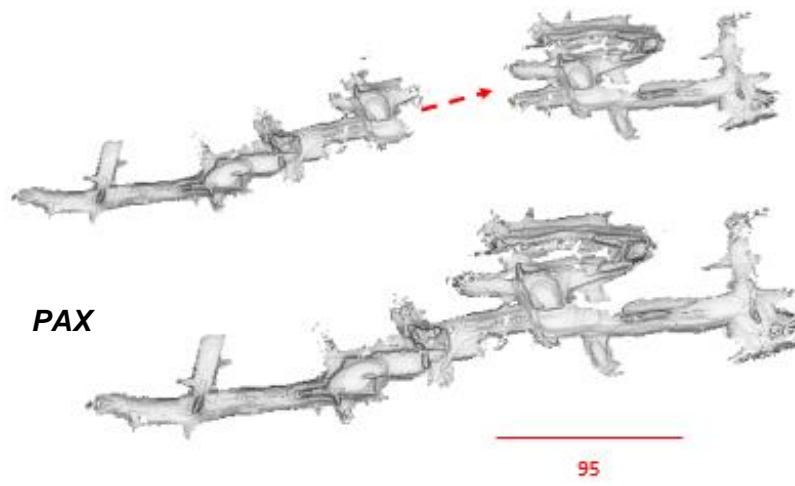
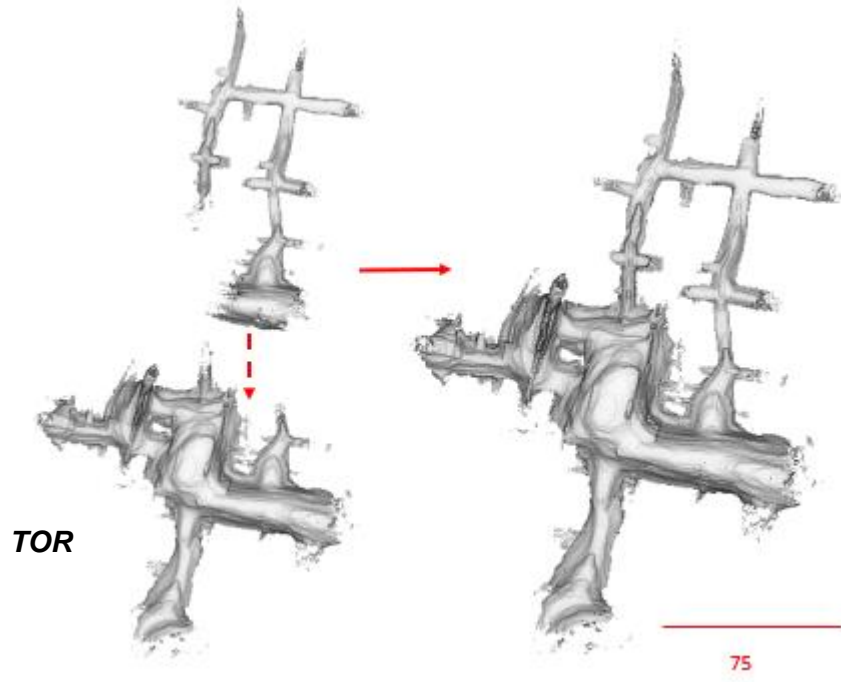
- [17] Kaiser, P.K., Tannant, D.D., McCreath, D.R., 1996. Canadian Rockburst Support Handbook. Geomechanics Research Centre, Laurentian University, Sudbury, Ontario, p.314.
- [18] Karmann, I. 1994. Evolução e dinamica atual do systema carstico do Alto Vale do Rio Ribeira de Iguape, sudeste do estado de São Paulo . Doctoral Thesis. Universidade do São Paulo, 228 pp.
- [19] Klimchouk, A., Ford, D.C., 2000. Lithologic and structural controls of dissolutional cave development. In: Klimchouk, A., Ford, D.C., Palmer, A.N., Dreybrodt, W. (Eds.), *Speleogenesis: Evolution of Karst Aquifers*. National Speleological Society, Huntsville, USA, pp. 54–64.
- [20] Klimchouk, A. (2007). *Hypogene Speleogenesis: Hydrogeological and Morphogenetic Perspective*. National Cave and Karst Research Institute.
- [21] Klimchouk, A. (2009). Morphogenesis of hypogenic caves. *Geomorphology*, 106(1–2), 100–117.
- [22] Klimchouk AB (2015). The karst paradigm: changes, trends and perspectives. *Acta Carsologica* 44(3):289–313.
- [23] Klimchouk, A., Auler, A. S., Bezerra, F. H. R., Cazarin, C. L., Balsamo, F., & Dublyansky, Y. (2016). Hypogenic origin, geologic controls and functional organization of a giant cave system in Precambrian carbonates, Brazil. *Geomorphology*, 253, 385–405.
- [24] LOUCKS, R.G., 2007. A review of coalesced, collapsed paleocave systems and associated suprastratal deformation. *Acta Carsologica*, 36 (1), 121-132.
- [25] Lowe, D.J., Gunn, J., 1997. Carbonate speleogenesis: an inception horizon hypothesis. *Acta Carsologica* 26, 457–488.
- [26] Misi, A., Kyle, J.R., 1994. Upper Proterozoic carbonate stratigraphy, diagenesis, and stromatolitic phosphorite formation, Irecê Basin, Bahia, Brazil. *J. Sediment. Res.* A64,299–310.
- [27] Misi, A., Kaufman, A.J., Azmy, K., Dardenne, M.A., Sial, A.N., Oliveira, T.F., 2011. Neoproterozoic successions of the São Francisco Craton, Brazil: the Bambuí, Una, Vazante and Vaza Barris/Miaba groups and their glaciogenic deposits. In: Arnaud, E., Halverson, G. P. and Shields-Zhou, G. (eds.) *The Geological Record of Neoproterozoic Glaciations*. Geological Society, London, *Memoirs*, 36, 509–522.
- [28] Palmer, A.N., 1991. The origin and morphology of limestone caves. *Geol. Soc. Am. Bull.* 103, 1–21.
- [29] White, W. B., Culver, D. C., & (2005). *Encyclopedia of caves*. Breakdown, Chapter 21.
- [30] Zlot, R., & Bosse, M. (2014b). Three-Dimensional Mobile Mapping of Caves. *Journal of Cave & Karst Studies*, 76(3).

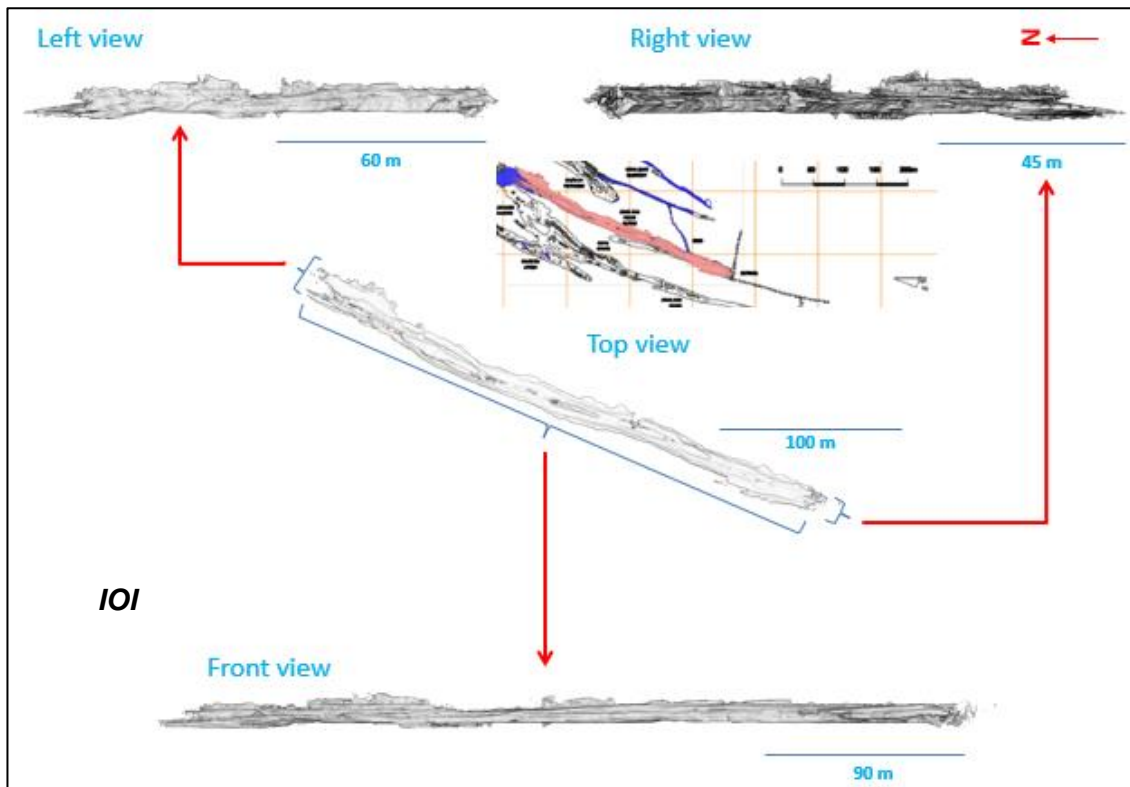
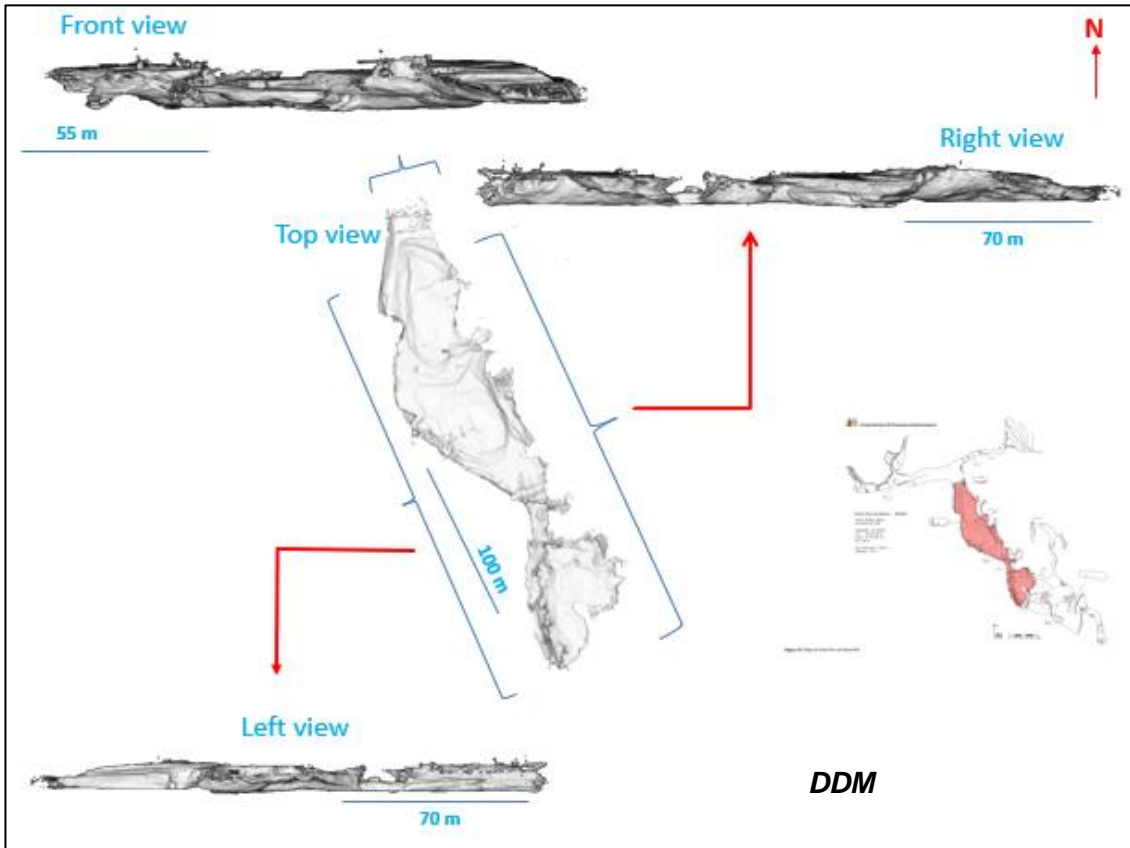


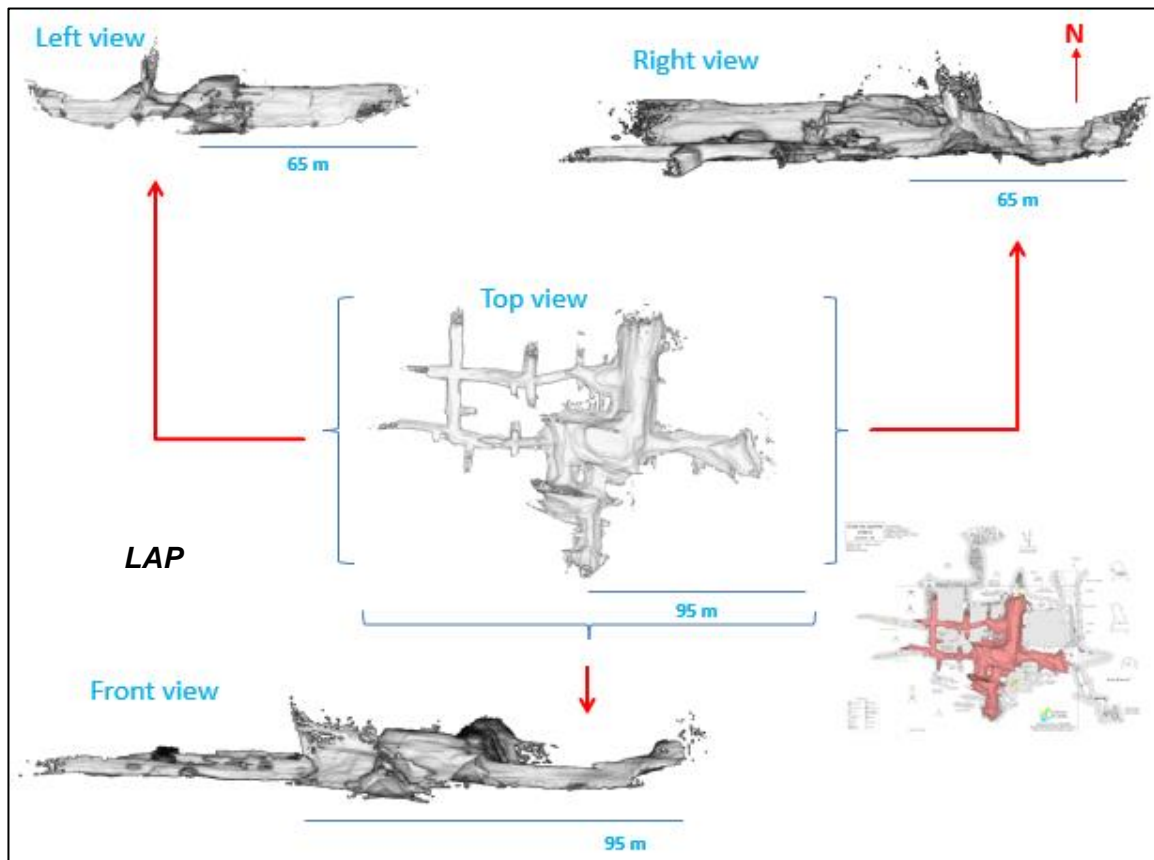
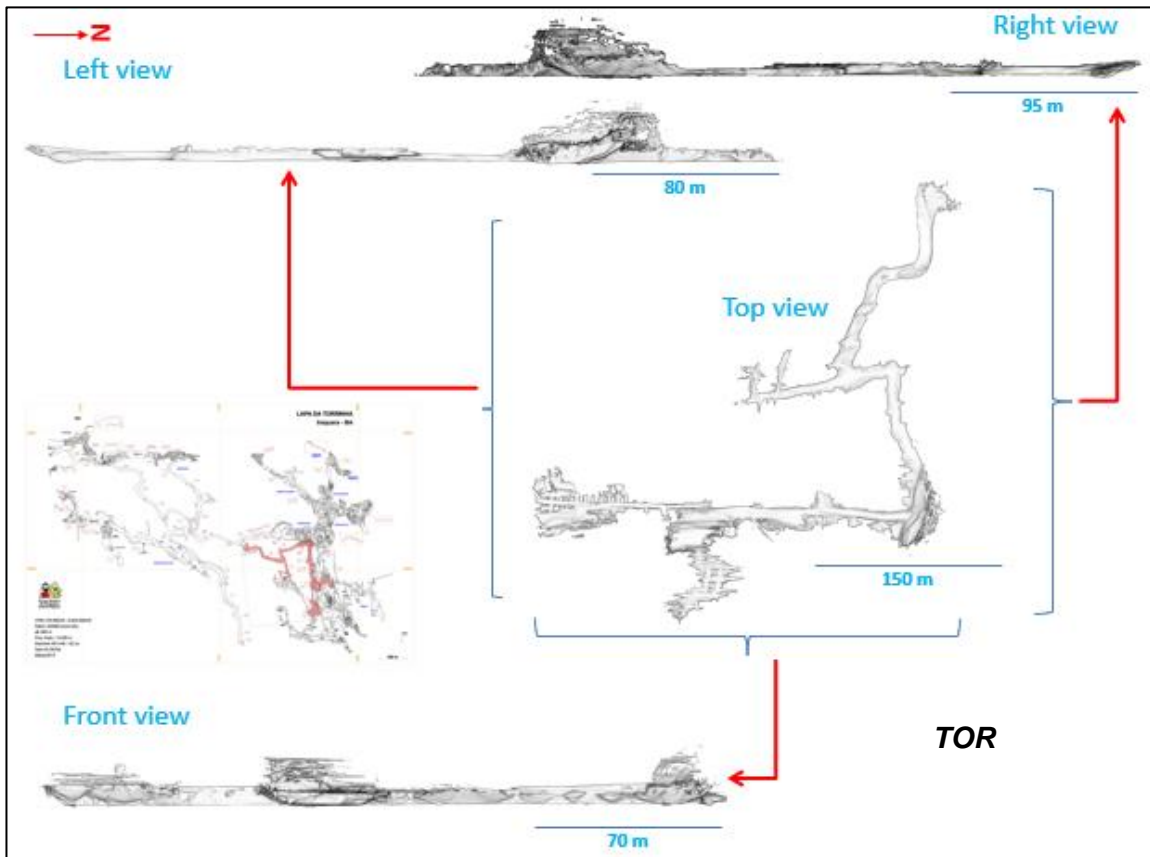


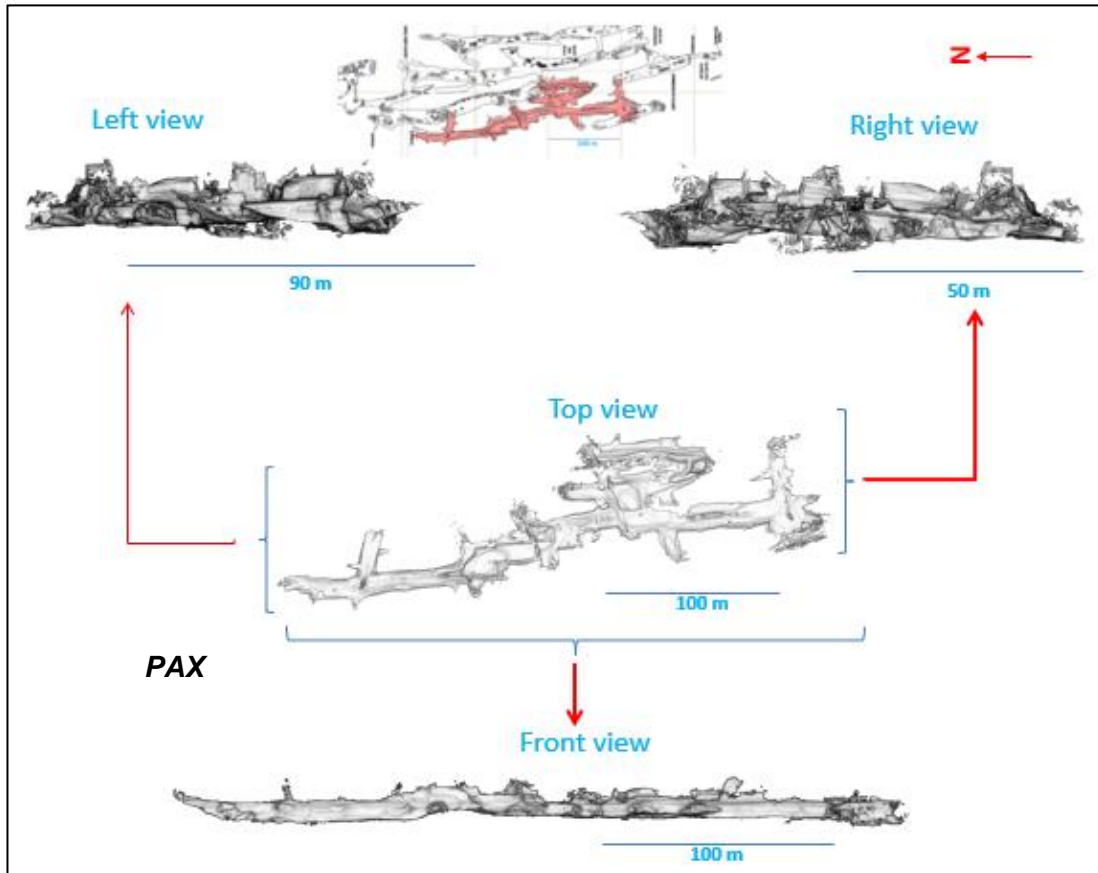
Appendix 2. Cave Point Clouds Alignment











Appendix 3. Aspect Ratios

<i>DDM</i>	<i>Width</i>	<i>Length</i>	<i>Aspect Ratio</i>
1	42.10	5.45	7.73
2	34.63	7.43	4.66
3	34.20	11.99	2.85
4	55.06	12.00	4.59
5	-	-	-
6	27.73	9.33	2.97
7	-	-	-
8	22.15	6.57	3.37

<i>IOI</i>	<i>Width</i>	<i>Length</i>	<i>Aspect Ratio</i>
1	-	-	-
2	-	-	-
3	13.02	6.22	2.1
4	13.2	6.30	2.06
5	15.72	4.81	3.27
6	16.28	6.25	2.61
7	13.31	7.29	1.82
8	12.37	7.77	1.59

9	17.04	6.50	2.62
10	12.80	7.47	1.71

<i>TOR- Part B</i>	<i>Width</i>	<i>Length</i>	<i>Aspect Ratio</i>
1	2.62	6.77	0.39
2	4.80	7.23	0.66
3	2.84	7.07	0.40
4	3.01	7.24	0.42
5	3.10	7.04	0.44
6	3.10	6.06	0.51
7	-	6.05	-
8	-	5.74	-
9	-	5.36	-
10	4.29	5.44	0.79
11	5.50	7.01	0.78
12	6.23	7.73	0.81

<i>TOR-Part B Maze</i>	<i>Width</i>	<i>Length</i>	<i>Aspect Ratio</i>
1	3.18	7.651	0.42
2	3.045	6.139	0.50
3	1.88	2.491	0.75
4	2.642	4.893	0.54
5	3.268	6.717	0.49
6	2.418	6.046	0.40
7	1.793	2.402	0.75

<i>TOR- Part A. A</i>	<i>Width</i>	<i>Length</i>	<i>Aspect Ratio</i>
1	10.23	2.591	3.95
2	7.80	2.818	2.77
3	8.41	2.515	3.34
4	11.15	2.534	4.40

<i>TOR- Part A. B</i>	<i>Width</i>	<i>Length</i>	<i>Aspect Ratio</i>
1	8.01	2.147	3.73
2	8.91	3.124	2.85
3	8.31	2.791	2.98
4	11.65	3.98	2.93
5	10.79	4.031	2.68

TOR-Part A.C	Width	Length	Aspect Ratio
1	7.92	3.35	2.36
2	11.82	3.49	3.38
3	13.00	3.88	3.35
4	6.17	2.75	2.24
5	6.12	2.97	2.06
6	5.72	3.01	1.90
7	5.21	3.02	1.72
8	-	-	-

TOR-Part A. D	Width	Length	Aspect Ratio
1	9.25	2.74	3.38
2	7.83	2.41	3.25
3	6.32	1.77	3.58
4	9.38	3.01	3.12

Appendix 4. Structural Data

DDM		
	Dip Direction	Dip Angle
Fractures	335	90
	332	90
	330	90
	340	90
	338	90
	16	90
	336	90
	325	90
	20	90
	250	90
Veins	248	88
	243	83
	240	79
	258	80
	235	75

IOI		
	Dip Direction	Dip Angle
Veins	165	85
	155	86
	180	82
	150	80
	158	87

	145	85
	163	84

TOR		
	<i>Dip Direction</i>	<i>Dip Angle</i>
<i>Fractures</i>	260	90
	255	90
	215	90
	260	90
	186	90
	250	90
	260	90
	257	90
	225	90
	230	90
	70	90
	69	90
	86	90
	80	90
	90	90
	65	90
	80	90
	83	90
	64	90
	355	90
	90	90
	87	90
	65	90
	88	90
	93	90
	260	90
	270	90
	272	90
	273	90
	265	90
	82	90
	87	90
	83	90
	79	90
	85	90
	75	90
	82	90
	75	90
	85	90
	80	90
83	90	

	80	90
	74	90
	74	90
	85	90
<i>Veins</i>	73	88
	262	85
	242	85
	284	88
	258	87
	250	87
	258	84
	91	86
	357	86
	262	88
	164	84
	352	88
	347	89
	84	87
	263	88
	246	78
	177	83
	263	74
	164	75
	236	79
	266	87
	251	79
	153	86
	73	88
	232	82
	259	89
	273	82
	271	87

<i>LAP</i>		
	<i>Dip Direction</i>	<i>Dip Angle</i>
	95	90
	105	90
	103	90
	93	90
	71	90
	103	90
	175	90
	160	90
	100	90
	100	90
	101	90

<i>Fractures</i>	165	90
	177	90
	60	90
	145	90
	180	90
	175	90
	163	90
	164	90
	179	90
	170	90
	187	90
	75	90
	2	90
	358	90
	278	90
	174	90
	342	90
	345	90
	12	90
	304	90
	276	90
	268	90
	198	90
	201	90
	353	90
	90	90
	352	90
	20	90
	86	90
	172	90
	83	90
	91	90
	276	90
	354	90
	92	90
	75	90
	92	90
	182	90
	359	90
	170	90
80	90	
9	90	
2	90	
10	90	
4	90	
345	90	
155	90	

Veins	92	89
	196	89
	198	87
	97	86
	183	88
	211	85
	3	85
	98	89
	90	89
	165	85
	345	82
	23	8
	1	70

PAX		
	Dip Direction	Dip Angle
Fractures	0	90
	280	90
	270	90
	170	90
	266	90
	180	90
	265	90
	257	90
	264	90
	282	90
	60	90
	265	90
	256	90
	253	90
	244	90
	253	90
	236	90
	157	90
	253	90
	76	90
	242	90
	259	90
	7	90
	242	90
	232	90
	334	90
	262	90
	68	90
	88	90
	85	90

	86	90
	84	90
	86	90
	89	90
Veins	162	82
	159	85
	78	89
	168	86
	184	89
	188	81
	158	86
	21	82

Appendix 5. Stability Analysis Contour Plots

